FUEL CELL CATHODE AIR FILTERS: METHODOLOGIES

FOR DESIGN AND OPTIMIZATION

Except where reference is made to the work of others, the work described in this thesis is my own or was done in collaboration with my advisory committee. This thesis does not include proprietary or classified information.

_____

Daniel Mabry Kennedy

Certificate of Approval:

_____	_____
Gopal A. Krishnagopalan Professor Chemical Engineering	Bruce J. Tatarchuk, Chair Professor Chemical Engineering
_____	_____
R. Mark Nelms Professor Electical Engineering	Joe F. Pittman Interim Dean Graduate School

FUEL CELL CATHODE AIR FILTERS: METHODOLOGIES FOR DESIGN AND OPTIMIZATION

Daniel Mabry Kennedy

A Thesis

Submitted to

the Graduate Faculty of

Auburn University

in Partial Fulfillment of the

Requirements for the

Degree of

Master of Science

Auburn, Alabama
May 10, 2007

FUEL CELL CATHODE AIR FILTERS: METHODOLOGIES

FOR DESIGN AND OPTIMIZATION

Daniel Mabry Kennedy

_____
Signature of Author

_____
Date of Graduation

THESIS ABSTRACT

FUEL CELL CATHODE AIR FILTERS: METHODOLOGIES

FOR DESIGN AND OPTIMIZATION

Daniel Mabry Kennedy

Master of Science, May 10, 2007
(B.S., Auburn University, 2004)

98 Typed Pages

Directed by Bruce Tatarchuk

Platinum catalyst used in PEM fuel cells experience performance degradation such as reduction in efficiency and life as a result of airborne contaminants. Research on these contaminant effects suggests that the best possible solution to allowing fuel cells to operate in contaminated environments is by filtration of the harmful contaminants from the cathode air. A cathode air filter design methodology was created that considers the properties of the cathode air stream, fuel cell attributes, and filter options to optimize the filter design process. Optimization of the filter requires an understanding of the balance that must be made between the loss in power due to poisoning of the platinum catalyst and a loss in fuel cell efficiency created by an increase in parasitic power required to operate the compressor. The model was successfully applied to a 1.2kWe fuel cell. Results show that the optimal filter design is dependent on both the total logs of removal required and the total capacity required. A novel filter media, microfibrous materials,

provides the thinnest possible bed depth and lowest parasitic power requirements for cases requiring high logs removal and low capacity. Packed beds provide the best solution for high inlet concentrations and/or long breakthrough time applications. If both a high contacting efficiency and capacity are required, an optimized composite bed provides the ideal solution by utilizing the advantages of both filter types.

Style Manual Used: Chemical Engineering Progress Style Guide, available at www.cepmagazine.org/editorial/refstyle.htm

Computer Software Used: Microsoft Word, Microsoft Excel, Microsoft PowerPoint, Pro-RAE Suite, Maple 7.0

TABLE OF CONTENTS

LIST OF TABLES

LIST OF FIGURES

I. INTRODUCTION

Fuel cells are being actively considered for a wide range of applications including automobiles, uninterruptible power supplies, and battery replacements in the military for dismounted soldiers [1]. The reason for the interest in fuel cells is owed to their high power densities, low operating temperatures, low emissions, quiet operation, and their potential for system robustness [2]. However, air in these operating environments may contain contaminants that are damaging to fuel cell performance such as carbon monoxide, sulfur compounds, and volatile organic compounds (VOCs). It has been suggested that the best method for addressing fuel cell air contamination is by the inclusion of adsorptive filtration with a cathode air filter [3]. Filters used in fuel cells must be optimized to be durable and effective, as well as easily adaptable to each specific need. Optimization of cathode filter design requires careful consideration of fuel cell operating variables and available filter technology**.** These design considerations were studied in detail and organized to create a process that provides a blueprint for designing and optimizing cathode air filters capable of allowing fuel cells to be operated in contaminated environments.

Research on the durability of proton exchange membrane fuel cells has typically focused on the effects and the remediation of the effects of chemical contaminants on the hydrogen electrode, or anode. This focus has been driven primarily by the intent to use

reformed hydrogen from fossil fuels containing contaminants toxic to the sensitive platinum catalyst. However, due to the higher complexity of the oxygen reduction reaction when compared to reduction of hydrogen at the anode, the oxygen electrode, or cathode, requires twice the platinum (0.1 mg cm^{-2} as compared to 0.05 mg cm^{-2}) and is therefore potentially more sensitive [4]. Recent studies have confirmed that polluted or otherwise contaminated environments negatively affect the performance of proton exchange membrane fuel cell cathodes. For example, 20 ppm of carbon monoxide causes a temporary 4% reduction in fuel cell output. Other contaminants, for example sulfur compounds such as H_2S and SO_2, cause a more permanent effect reducing performance to as low as 30% of original output [3, 5].

Two methods for dealing with contaminated air effects on fuel cell cathodes are to increase catalyst durability and/or to filter contaminants from the air. Because of the wide variety of contaminants, increasing membrane resilience by modifying the catalyst or increasing the catalyst amount is a difficult and possibly expensive alternative. Therefore, the most effective and flexible method for operating fuel cells in contaminated environments is adsorptive filtration of contaminants from the ambient air stream.

The wide variety of filtration technology options allows for tailoring of cathode air filters to different contaminant types and concentrations. Optimization of filter design requires a methodology incorporating air properties, fuel cell attributes, and design options. A better understanding of how a cathode air filter should perform is accomplished through a detailed study of the design considerations and how they affect each other.

II. BACKGROUND INFORMATION

1. Fuel Cells

Interest in fuel cell technology has increased dramatically in the last 20 years, driven primarily on concerns about the condition of the environment and sources of energy. The increase in world population and per capita energy requirements has led society to search for sources of energy that are both efficient and environmentally friendly. Goals of energy research focus on energy creation that produces fewer and less harmful gases than traditional combustion which currently provides most of the world's power. Fuel cells potentially meet both environmental and efficiency goals. Fuel cells operate by continually converting chemical energy to electrical energy through a reverse-electrolysis process as long as fuel and oxidant are supplied. One of the most common types of fuel cells, proton exchange membrane fuel cells (PEMFCs), uses hydrogen as a fuel source and produces only water as a byproduct. PEMFCs are therefore considered a zero emission engine. Compared to combustion engines, fuel cells are far more efficient due to the fact that they are not limited by the Carnot Efficiency. Due to their low emissions, quiet operation and high power densities that they provide, there is a large focus to apply fuel cells to a variety of applications ranging from laptops to unmanned aerial vehicles [6].

1.1. Fuel Cell Applications

Although the process by which fuel cells operate has been understood since 1839, the first practical application of fuel cells wasn't until the space program during the 1960's. NASA used fuel cells as power generators and as a water supply for the Gemini and Apollo space vehicles. Over the last few decades development of fuel cells has reached a level where they are now being studied for numerous applications. Phosphoric acid fuel cells (PAFCs), molten carbonate fuel cells (MCFCs) and solid oxide fuel cells (SOFCs) are all researched as a co-generator along side current electrical power plants [3]. Proton exchange membrane fuel cells, also known as polymer electrolyte membrane fuel cells, show promising potential for more varied applications such as transportation, uninterruptible power supplies (UPS), and small portable power devices (laptops, cell phones, PDAs,) as a battery replacement. Because of their low environmental impact, high power density, high conversion efficiency (50-55%), and long runtime capabilities, PEMFCs also show promise as electrical generators for users requiring reliable and high quality energy like hospitals, computer networks, and remote applications such as satellite dishes and communication towers. PEM fuel cells are also the most practical fuel cell type for application as domestic or residential generators. Military interest in using fuel cells ranges from unmanned aerial and underwater vehicles, portable battery chargers, and a replacement for batteries as a power source for dismounted soldiers, soldiers who fight on foot. Dismounted soldiers increasingly rely on electronic technologies such as computers, personal radios, global positioning systems, head up displays and thermal imaging. As battery technology nears its limit of technological

development, it can no longer provide soldiers with necessary power at an acceptable weight [7].

Several companies currently research and produce prototype PEM fuel cells for commercial and residential applications. Ballard has recently introduced a hydrogen powered stationary fuel cell power generator for use as an uninterruptible power supply in telecommunication markets. The NEXA RM series is a modular 1 kWe fuel cell designed to meet a range of power requirements depending on its specific application [1]. The base model NEXA fuel cell is a 1200 watt DC power supply operating on 99.9% pure hydrogen and clean air, while producing only water as a by product [8].

1.2. Proton Exchange Membrane Fuel Cell Technology

The chemical reaction in PEM fuel cells is the same as that in combustion of hydrogen.

$$2H_2 + O_2 \rightarrow 2H_2O \qquad \text{(II.1)}$$

The difference is instead of heat being produced causing thermal expansion, electrical current is generated. By creating electricity directly instead of through utilization of a combustion/expansion process, limitations described by the Carnot efficiency are removed, creating an increase in overall efficiency.

There are two steps for this reaction to complete and an electrical current to be generated. First, at the anode, hydrogen is ionized forming H^+ and electrons.

$$2H_2 \rightarrow 4H^+ + 4e^- \quad \text{(Eq. II.2)}$$

Second, at the fuel cell cathode, oxygen reacts with the hydrogen, using the electrons, to form H_2O.

$$O_2 + 4e^- + 4H^+ \rightarrow 2H_2O \quad \text{(Eq. II.3)}$$

The key to the production of electricity is the polymer membrane between the anode and cathode. The membrane is specifically designed to allow only the proton and not the electrons to pass through [9]. The electrons are required to follow a circuit potentially through a load to reach the hydrogen and oxygen reaction.

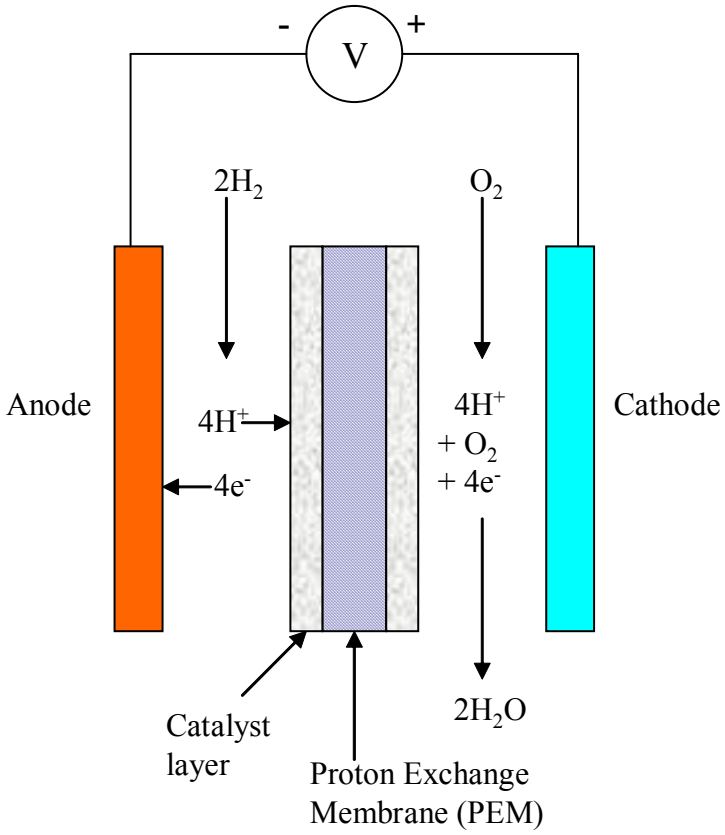

Figure II.1: A picture of a proton exchange membrane

1.3. Contaminant Effects on Fuel Cell Performance

Providing a clean fuel for fuel cells is important, especially for fuel cells using a sensitive polymer electrolyte membrane. The amount of research and published papers focusing on clean fuels supports this idea. In many cases the hydrogen for PEMFCs is provided by reforming heavy hydrocarbons. This leaves a large amount of contaminants

in the hydrogen stream that must be removed before supplied to the fuel cell. However, in recent years, researcher attention has moved from an almost exclusive focus on purifying hydrogen for fuel cell anodes, to also attempting to understand and remediate effects of contaminants in the oxidant provided to fuel cell cathodes. Contaminant effects on fuel cell cathodes becomes very important when considering the intended applications of fuel cells ranging from polluted city centers to dusty battlefields. For this reason, research began studying the effects of impurities on fuel cell performance to access the durability and capability of fuel cells to operate in more harsh environments than those found in a laboratory. The following table has been compiled from several sources on the effects of various contaminants on the current output of the fuel cell. Values of the percentage of normal current output were recorded both during challenge of the contaminant gas and following a flow of clean air which was provided until steady state has been achieved.

Table II.1
A list of contaminants and their steady-state effects on fuel cell power output during operation with contaminants air and operation after using clean air

Contaminant	Concentration	Percentage Output During Challenge	Percentage Output After Recovery	Source
Carbon Monoxide	20 ppm	96%	100%	[2]
Sulfure Dioxide	0.5 ppm	90%	90%	[2]
	2.5 ppm	47%		[10]
	5.0 ppm	22%	35%	[10]
Benzene	50 ppm (50mA/cm^2)	95%	95%	[2]
	50 ppm (100mA/cm^2)	93%		[2]
	50 ppm (200mA/cm^2)	72%		[2]
Sulfur Mustard	15 ppm	13%	13%	[2]
Sarin	170 ppm	30%	30%	[2]
H_2S	200 ppm	10%	30%	[10]

The effect of sulfur and organic compounds on fuel cell output has been correlated not only to its concentration, but also total dosage. This is primarily due to its more permanent, poisoning effect [11]. Recovery of the fuel cell from sulfur adsorbed on the platinum catalyst must be achieved by cyclic voltammetry which oxidizes the sulfur releasing it from the platinum catalyst. Cyclic voltammetry is a possible method of dealing with the effect of sulfur compounds on fuel cells; however, the equipment is expensive making pre-emptive filtration a more suitable means of dealing with contaminants [11]. Research on the effects of heavier VOCs and nerve agents at levels that might be associated with the release of a chemical agent in warfare conditions has revealed a gradual yet non-recoverable effect of these contaminants on the catalyst. The conclusion from research on the contaminant effects on fuel cells is that, if ambient air is used as an oxidant source, mitigation against exposure to contaminants will most likely

involve the use of some filtration device rather than an increase in tolerance of the fuel cell catalyst [2].

2. Adsorption

Adsorption occurs when one or more components of a gas or liquid are attracted to a solid adsorbent become lightly and sometimes reversibly bonded. This attraction is sometimes called van der Waals adsorption [12]. The fluid is continually passed through a fixed bed until the solid particles become saturated or are no longer able to remove desired components at an acceptable rate. Applications of gas phase adsorption include removal of volatile organic compounds (VOC's), sulfur compounds, and odors from air.

Adsorbents have a large surface area to volume ratio by containing pores that typically reach up to 50% of total volume. This results in surface areas of 100 to 2000 m^2/g. Activated carbon is a commonly used adsorbent for organic molecules. It is a microcrystalline material made by thermal decomposition of wood, vegetable shells, and other organic solids. The resulting material has surface areas of 300 to 1200 m^2/g and average pore diameters of 20 to 60Å. Other common adsorbents include silica gel, activated alumina, molecular sieve zeolites, and synthetic polymers of resins [12].

3. Microfibrous Materials

Microfibrous materials are a patented class of materials developed at Auburn University that possess several advantageous properties when used for catalyst or sorbent applications. They are composed of a sinter-locked network of micron diameter fibers made out of either polymer, metal, or ceramic and used to entrap catalysts/sorbent particulates. Particulates entrapped in the materials are far smaller (158 μm) than those used in a packed bed (765 μm) creating a more accessible surface area. Static mixing

adds to the contacting efficiency and is the result of flow around the fibers reducing intrapartical heat and mass transfer resistance. Therefore, when microfibrous materials are applied as a reaction/sorption system, they exhibit superior contacting when compared to monoliths and packed beds [8].

The process of preparing microfibrous materials involves mixing a slurry of micron diameter fibers with pulped cellulose and selected particulates (sorbents or catalyst supports). This slurry is then cast into a sheet using a wet lay process and then sintered to remove cellulose binder and to entrap the particulates in a sinter-locked network of fibers. This can be accomplished on well understood traditional high speed, low cost paper making equipment resulting in high uniformity of basis weight. The end product exhibits unique properties in terms of void volume, conductivity, porosity, surface area, permeability, and particle size [8].

Figure II.2: Three rolls of microfibrous materials using fibers made of ceramic, metal, and polymers

The fibers can be made of metal, polymer or ceramic, each possessing its own advantages. Metal fibers are conductive which allows the sheet to be applied as an electro catalyst or for electrical swing adsorption. Metal fibers are also able to withstand temperatures high enough for temperature swing regeneration of sorbents. Polymer fibers are low cost and an option for disposable filters such as home HVAC or cathode air filters; however, these fibers are for relatively low temperature applications only and unable to be temperature regenerated. The flexibility of the polymer also makes them good candidates for pleating. Ceramic fibers are resistant to caustic environments and heat. Figure 2.4 shows a micrograph of the three different fiber types sintered to hold particulates.

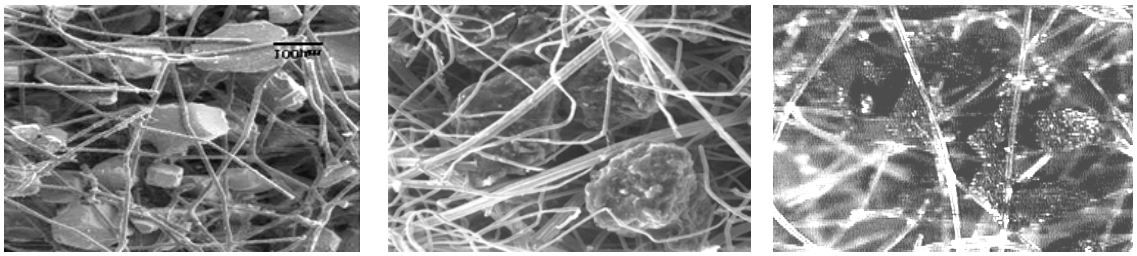

Figure II.3: A micrograph showing the three types of microfibrous materials and supported sorbents

High voidage (70-95%) and extremely small particle size (as low as 50 micron in diameter) used in microfibrous materials creates static mixing thereby reducing intraparticle mass transport resistance [3]. With adjustments of fiber diameter and particle size, surface kinetics of the reaction can be matched with the heat and mass transport at the reaction site. Optimization of the materials results in a higher contacting efficiency and lower pressure drops.

The high contacting efficiency of microfibrous materials results in high sorbent utilization. However, microfibrous materials have low sorbent loading when compared to a packed bed. Packed beds have high volumetric loading and but have a comparably lower contacting efficiency [3]. By adding a layer of microfibrous materials downstream of a packed bed, a composite bed is created utilizing packed bed sorbent loading and microfibrous material contacting efficiency. A composite bed synergistically combines the advantages of the a packed bed with those of the microfibrous 'polishing' layer to create a thinner more efficient filter bed capable of high logs of removal of contaminants. Further understanding and modeling of the composite bed can be accomplished with the equal areas design rule [13].

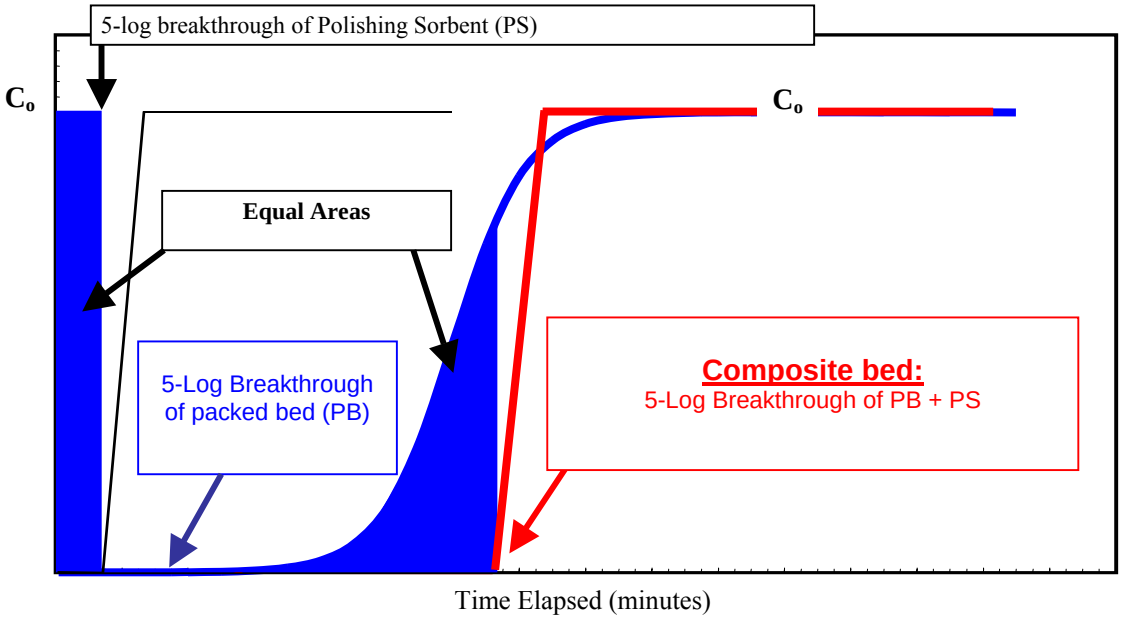

Figure II.4: Diagram showing benefit of composite bed

This plot shows the increase of breakthrough time by adding a microfibrous polishing layer to the exit of a packed bed. The sigmoidal breakthrough curve of the packed bed shows its lack of sorbent utilization and inability to continue a high log removal once breakthrough occurs. Conversely, the sharp breakthrough curve of microfibrous materials represents the high contacting efficiency and sorbent utilization before breakthrough. By adding this layer to the end of a packed bed, the capacity of the microfibrous layer is used to remove contaminants breaking through the packed bed therefore causing a sharper breakthrough curve. This causes a higher overall sorbent utilization and extends the high log breakthrough time two to three times. This allows for an overall thinner filter design with lower catalyst/sorbent requirements [13].

III. EXPERIMENTAL APPARATUS

1. Ballard NEXA Fuel Cell

A NEXA power module, produced by Ballard Power Systems, is a small automated fuel cell system designed for portable and back-up power applications. The system uses a polymer membrane electrolyte, with a platinum catalyst layer. It uses hydrogen as a fuel and oxygen from air as an oxidant. This fuel cell design results in a system that is very quiet and produces zero harmful emissions (only water and heat), allowing for indoor operation. Fuel cell operation is designed to be continuous as long as hydrogen is provided. The system provides 1200 watts of DC power output at a nominal output voltage of 26 VDC. Figure III.1 shows a picture of the system [8].

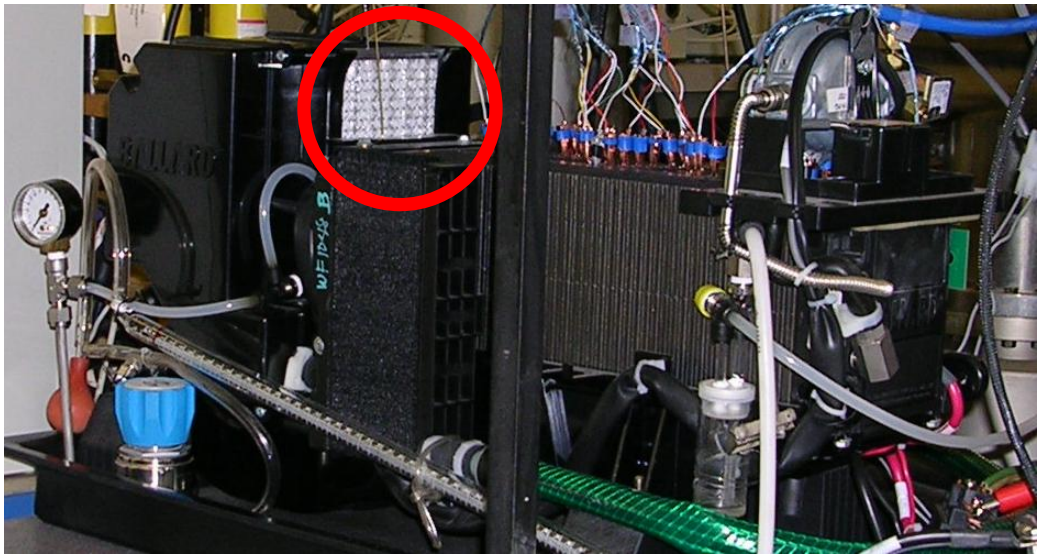

Figure III.1: Picture of Ballard NEXA Fuel Cell with the cathode air filter circled

The system is comprised of four parts: a Ballard fuel cell stack, hydrogen delivery, oxidant air supply, and cooling air supply. Onboard sensors monitor system performance while a control board automates fuel cell operation. Battery power is required for start up and shutdown requirements [8].

The NEXA fuel cell has been optimized for the portable power market. It operates at low pressure, minimizing parasitic power loss, reducing noise, and enhancing system reliability. Also, the stack does not require external fuel humidification. A humidity exchanger controls humidity in the cathode air by exchanging water from the exhaust from the cathode [8].

Oxygen is provided to the stack by a small compressor. The compressor speed is variable, allowing for an optimized flow of oxygen to meet system power demand. An

intake filter is required to protect the compressor and fuel cell stack from particulates and chemical contaminates [8].

Fuel cell stack temperature, hydrogen pressure, hydrogen leak concentrations, stack current, stack voltage, air mass flow, and purge cell voltage are monitored by input signals to the control board. The controls then output a pass/fail check based on operations status. Depending on the severity of the situation, the fuel cell will either attempt to remedy the situation, set off an alarm, or execute a shutdown sequence [8].

2. Compressor Testing Apparatus

The compressor testing apparatus involves two replaceable orifice plates on each side of the compressor. The upstream orifice represents a pressure drop across a filter and the downstream represents system pressure drop through the stack, from the compressor outlet to atmospheric pressure. PVC pipes with a 1.5" ID were used to connect the compressor to hold the orifice plates. At the exit, a 2' long PVC pipe with a 0.5" hole in the 6 inches from the end of the pipe allows for insertion of an Extech hot wire anemometer. The pressure was recorded at the inlet and outlet of the compressor by inserting a needle into the rubber hosing connecting the compressor to flow expanders. Flow expanders were then connected to the PVC pipes and sealed with ducting tape. By recording values at the compressor inlet and outlet, rather than a traditional pressure tap at D and 0.5D before and after the orifice plates, pressure comparisons could be made with values recorded within the fuel cell system. The following picture shows the testing apparatus.

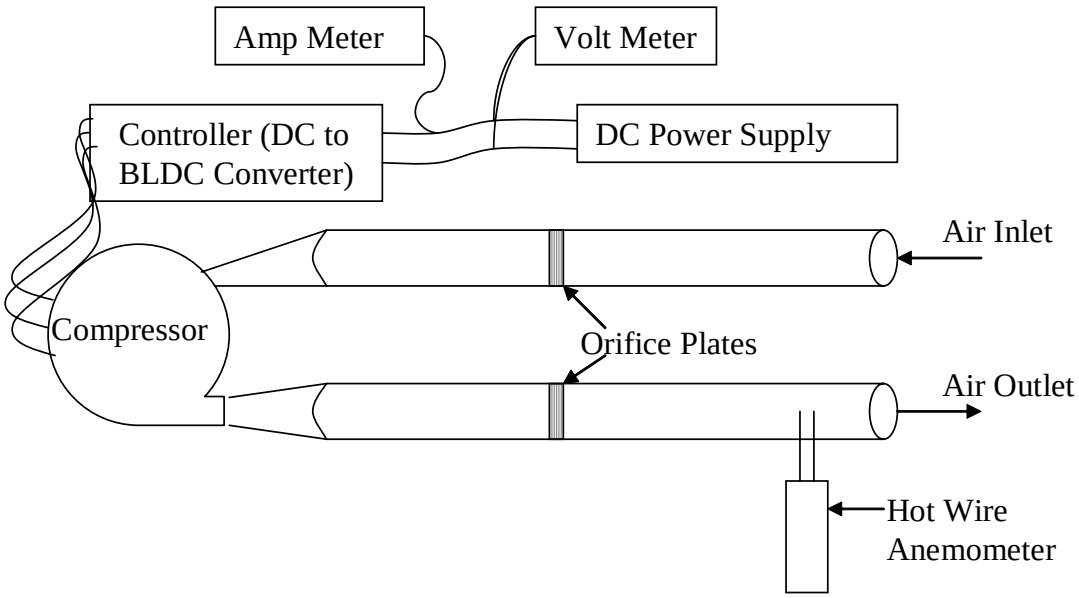

Figure III.2: Compressor testing apparatus used for testing the compressor outside of the fuel cell

Pressure was recorded on a 36" Dwyer manometer. Power to the motor was provided by a Lambda power supply model #LLS7060 capable of providing power at 0-60 volts at 4.8 amps. Power to the controller was provided by an Electro Industries Regulated power supply (model #3002A) capable of producing 0-30 volts at 2.5 amps. Voltages and amperages were confirmed using two fluke 87 multimeters and one fluke 77 multimeter. Total power to the system was provided by adding the power to each component.

A bread board controller was built to control compressor speed while providing access to voltage and amperage values used to drive the compressor and power the controller. A circuit diagram of the controller is shown in Figure III.3.

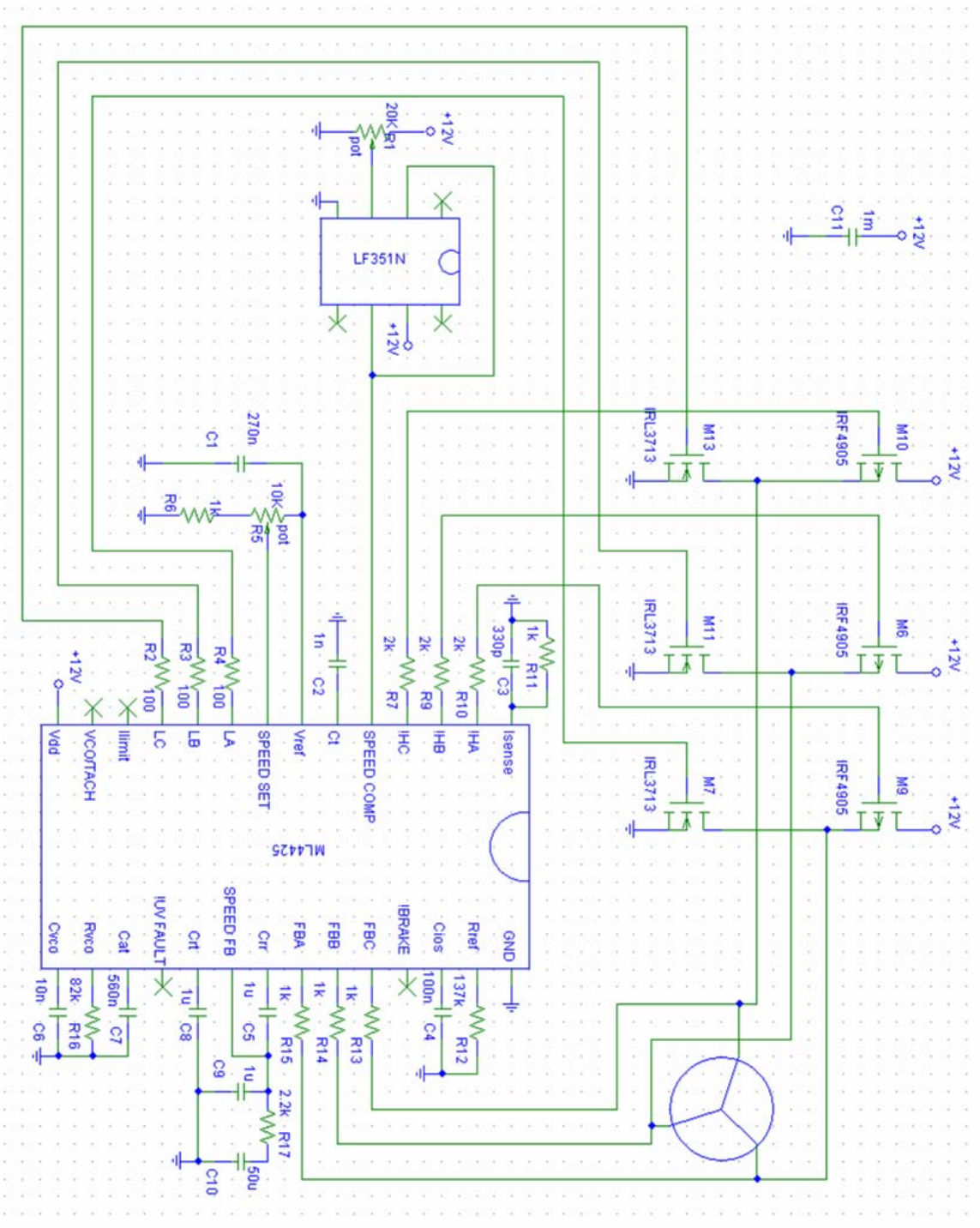

Figure III.3: Compressor controller diagram

3. Breakthrough Testing Apparatus

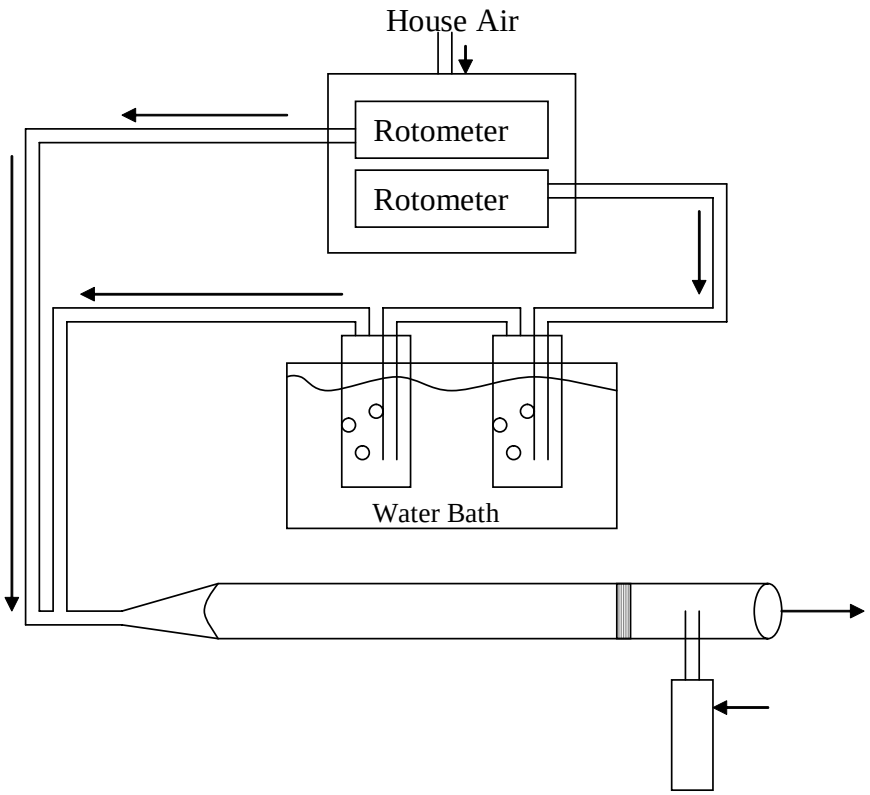

Figure III.4: Breakthrough testing apparatus

Figure III.4 shows the testing apparatus used in testing 2" circular samples of packed bed and microfibrous sheets. By modifying the exit portion of the apparatus, it was also possible to test the final filters used in the Ballard fuel cell.

The apparatus uses house air, which is split and controlled by two pairs of Omega rotometers. The first part passes through one of either a 0-500 ml/min or 0-7 ml/min rotometer and then passes through a two stage bubbler containing hexane. Only one rotometer was used at a time to maintain pressure and flow stability in the system. The bubblers were placed in a constant temperature water bath at 20^{o}C to ensure a constant hexane vapor pressure.

The other two rotometers control the bulk flow of air through the system using either a 0-150 SCFH or a 0-50 SCFH rotometer. This air combines with the air flowing through the hexane before it is run through the filter apparatus. The flow rate of the air through the hexane controls the final concentration of hexane in the system. The addition of the flow rates from both rotometers is the total flow rate through the filter.

The filter apparatus is a 2" id pipe with a 5' lead section providing time for the air to be well mixed and achieve a laminar flow regime. A 1' section after the filter provides a well mixed flow of air so that the concentration recorded at the exit represents and average concentration exiting the filter. Hexane concentrations were measured using a MiniRae PID detector.

For testing the full sized filters, a different filter holding device was constructed. Half of the device is shown is Figure III.5. There is a one foot inlet section containing a flow straightening device before air is run through the filter.

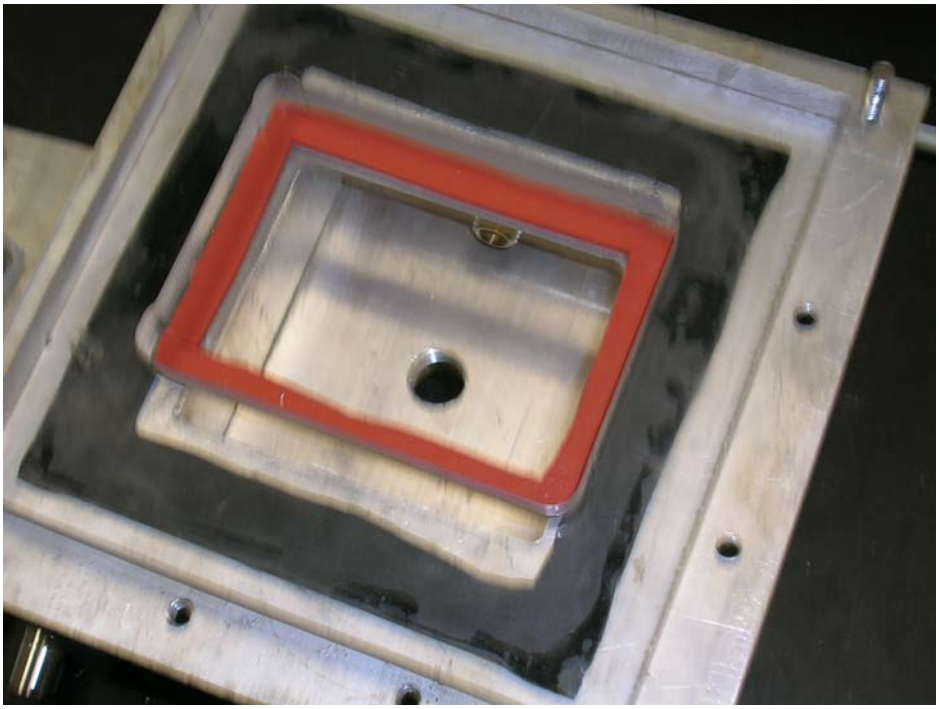

Figure III.5: Filter testing apparatus for testing filters that fit into a Ballard NEXA fuel cell

IV. DESIGN METHODOLOGY AND ALGORITHM

1. Fuel cell system design discussion and design considerations

1.1. Fuel cell system discussion

Optimization of cathode air filtration requires addressing a unique set of challenges present in the fuel cell system, shown in Figure IV.1. One such challenge is how to minimize the loss in efficiency caused by chemical contaminants poisoning the cathode section catalyst. A cathode air filter can be used to remove these contaminants; however, it causes an increase in system pressure drop, presenting yet another challenge. This pressure drop causes an increase in the required amount of pressure-volume work that the compressor must perform. An energy balance must be made between the loss in power due to poisoning of the platinum catalyst and a loss in fuel cell efficiency created by an increase in parasitic power required to pump air through additional filtration.

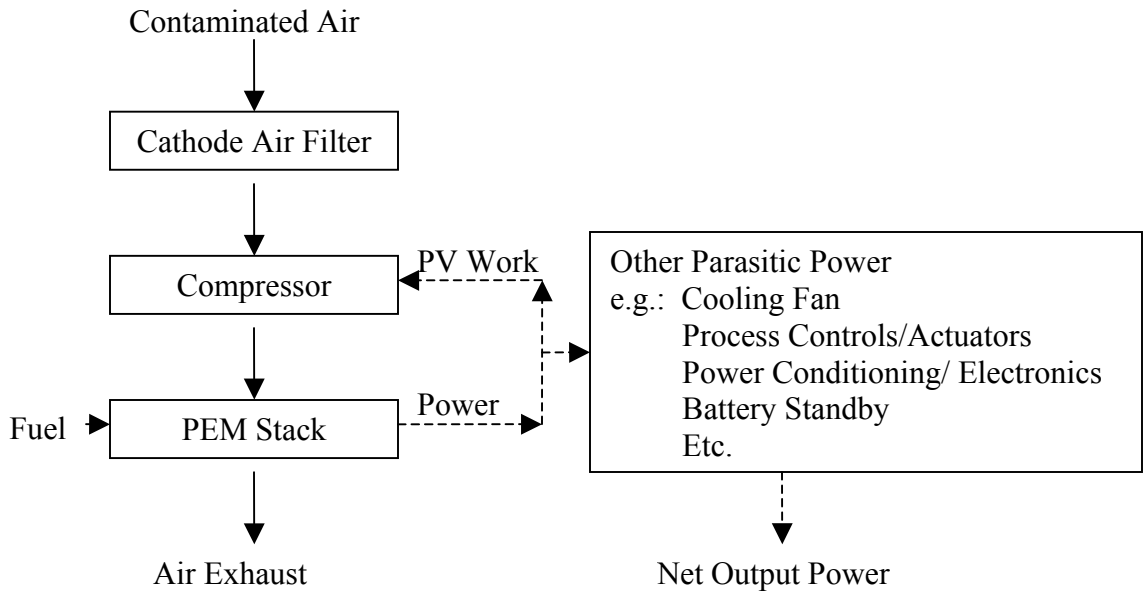

Figure IV.1: Fuel cell mass and energy balance showing the flow of air and power through the system

1.2. Filter design considerations

Cathode air filter design considerations fall into six categories: inlet air properties, adsorptive filter parameters, compressor attributes, stack attributes, filter footprint, and filter design options. Figure IV.2 shows how the design considerations are further broken down into individual variables within the filter and fuel cell system.

From this methodology, there are three categories of variables to consider: inlet air properties, filter design options, and filter footprint. Each of these categories can be further broken down into individual variables which can be studied for its effect on the compressor, stack, and ultimately the total fuel cell's performance. The effects of each of these categories are tied together with the adsorptive filter parameters: saturation capacity, removal efficiency, and pressure drop. These parameters then influence the PV

work required to operate the compressor at the desired air flow rate and the stack efficiency defined by the poison tolerance and lifetime.

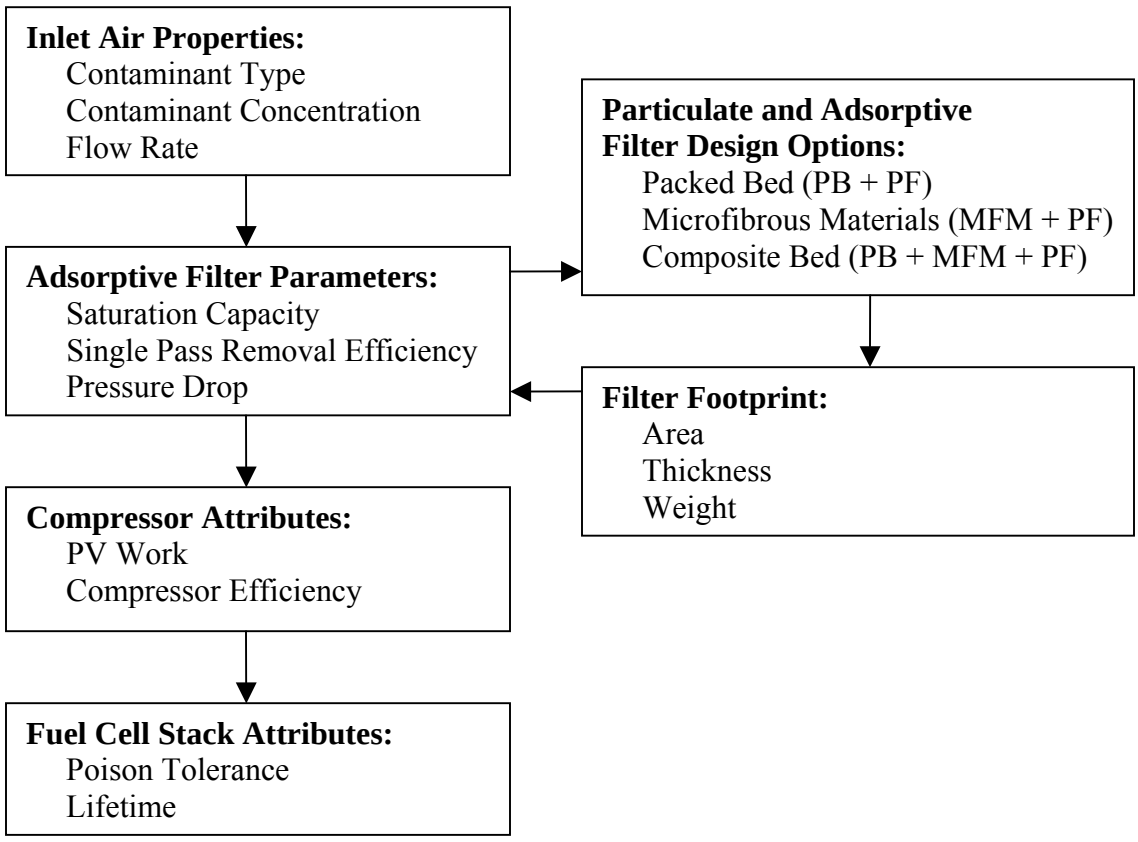

Figure IV.2: Hierarchal design considerations for cathode air filters

1.2.1. Inlet air properties

The inlet air properties, along with the stack attributes, dictate the efficacy and capability that the filters must possess. Air properties affect filter parameters by defining the capacity and removal efficiency needed to remove contaminants to achieve a specified output level. Single pass removal efficiency is increased by reducing adsorbent particle size thereby increasing surface area and eliminating intra-particle mass transport. High single pass removal efficiency results in a filter effective at removal of

contaminates at low concentrations. An increase in either the capacity or the removal efficiency results in an increase in both filter pressure drop and the amount of power required by the compressor.

1.2.2. Filter design options

While many filter design options exist, for this research three options are considered: packed bed (PB), microfibrous materials (MFM), and composite bed (MFM + PB). A packed bed is the most widely used form of filtration. Packed bed characteristics include high sorbent capacity, low single pass removal efficiency, and low pressure drop. The second design option, microfibrous materials, has been proven effective with high log and high single pass removal of chemical contaminants, but has a lower capacity and higher pressure drop when compared to packed beds. Microfibrous materials also add a new dimension to the problem, through application as a pleated filter media, or as a polishing sorbent in a composite bed formation [6]. Pleated microfibrous materials have an increased capacity and lower pressure drop than a flat sheet with a smaller area. A composite bed effectively combines the capacity of a packed bed and the high contacting efficiency of microfibrous materials. An optimized composite bed is capable of higher logs of removal, has a reduced total bed depth, and has a lower pressure drop than a packed bed.

1.2.3. Filter footprint

The last category that needs to be considered for its effect on filter parameters is the filter footprint. An increase in area allows for a decrease in thickness and visa versa.

In many cases, the footprint may be set by the fuel cell system in order for the filter to be retrofitted into the existing particulate filter slot. Filter weight affects the filter capacity and is required for analysis because of the differences in densities of the filter design options.

1.2.4. Adsorptive filter parameters

Inlet air properties, filter design options, and filter footprint all relate to the adsorptive filter parameters. Contaminant type, concentration, and flow rate affect the filter parameters by virtue of the differences in chemical properties that various contaminants have in relation to the filter adsorptive materials. Filter design options control the mass and energy transport properties of the filter by affecting contacting regimes as well as pressure drop. Lastly, the filter footprint affects all three filter parameters through bulk design.

1.2.5. Compressor attributes

Once the adsorptive filter parameters have been established, their effect on the compressor can be established. Pressure drop across the filter causes a decrease in inlet pressure (P_1) to the compressor creating a vacuum. The outlet pressure (P_2) from the compressor is set by the required flow rate necessary to operate the fuel cell. This increase in pressure ratio (P_2/P_1) across the compressor causes a decrease in compressor efficiency and an increase in compressor power. Both of these effects cause an overall decrease in fuel cell operating efficiency and performance.

1.2.6. Fuel cell stack attributes

The fuel cell stack is also affected by variations in the filter parameters. The stack has a certain tolerance and operating lifetime related to the concentration of contaminants passing through the cathode of the cells. The filter controls this concentration by reducing the contaminant concentrations before they make contact with the cathode. The single pass removal efficiency required is dictated by the maximum concentration tolerable by the fuel cell. The maximum concentration may be lower if the contaminant collects in the stack rather than passing through the exhaust.

Research on cathode durability has concluded that the effect that contaminants have on fuel cell performance varies depending on the contaminant type and concentration, leading to three different scenarios for contaminant remediation. In the first scenario, contaminants have little to no permanent effect, and do not build up in the system, so can be ignored. For example, it may be more acceptable to allow a small percentage of contaminant through, rather than to increase filtration, thereby resulting in a higher pressure drop. An example of this would be CO, where the damaging effect is both small and temporary.

In the second scenario, contaminants need to be completely removed, because any amount of exposure to the contaminant will cause a permanent degradation of fuel cell performance. These contaminants build up in the system, causing more severe degradation with longer exposure times. For example, a cathode air filter must be capable of removing sulfur compounds such as H_2S and mustard gas($C_4H_8Cl_2S$).

In the third scenario, contaminants must be removed to a point of maximum concentration to minimize a decrease in fuel cell performance. A decision for further

removal beyond this defined maximum must take into account the effect the increase in filter pressure drop will have on the system. For example, SO_2 at concentrations of 2.5-5 ppm has a significant effect on fuel cell performance, with as much as a 50 to 60% reduction in fuel cell power [4]. This situation would clearly require a cathode air filter for efficient fuel cell operation. SO_2 concentrations of lower than 0.5 ppm may be ignored completely as they have no noticeable effect [3], so a cathode air filter would not be necessary. However, at moderate concentrations, between 1 and 2 ppm, filtration design can be optimized between fuel cell performance and the effects of the increased filter pressure drop from additional filtration.

1.3. Cathode air filter optimization: a trade off between compressor power requirements and efficiency losses from catalysts poisoning

Research on cathode durability has concluded that the effect that contaminants have on fuel cell performance varies depending on the contaminant type and concentration, leading to three different scenarios for contaminant remediation. In the first scenario, contaminants have little to no permanent effect, and do not build up in the system, so can be ignored. For example, it may be more acceptable to allow a small percentage of contaminant through, rather than to increase filtration, thereby resulting in a higher pressure drop. An example of this would be CO, where the damaging effect is both small and temporary.

In the second scenario, contaminants need to be completely removed, because any amount of exposure to the contaminant will cause a permanent degradation of fuel cell performance. These contaminants build up in the system, causing more severe

degradation with longer exposure times. For example, a cathode air filter must be capable of removing sulfur compounds such as H_2S and mustard gas($C_4H_8Cl_2S$).

In the third scenario, contaminants must be removed to a point of maximum concentration to minimize a decrease in fuel cell performance. A decision for further removal beyond this defined maximum must take into account the effect the increase in filter pressure drop will have on the system. For example, SO_2 at concentrations of 2.5-5 ppm has a significant effect on fuel cell performance, with as much as a 50 to 60% reduction in fuel cell power [5]. This situation would clearly require a cathode air filter for efficient fuel cell operation. SO_2 concentrations of lower than 0.5 ppm may be ignored completely as they have no noticeable effect [3], so a cathode air filter would not be necessary. However, at moderate concentrations, between 1 and 2 ppm, filtration design can be optimized between fuel cell performance and the effects of the increased filter pressure drop from additional filtration.

2. Design equations for describing fuel cell attributes and filter parameters

The following design equations provide mathematical relationships that relate the design considerations to each other. These sections include equations for determining the required air flow rate to meet fuel cell power requirements, breakthrough time based on capacity and adsorption efficiency, pressure drop based on thickness, and compressor power based on inlet and outlet pressures.

2.1. Fuel cell air flow requirements

The required oxygen flow rate to operate a fuel cell can be found by the number of faradays provided by a mole of oxygen. Through substitution and simplification the following equation is derived [2].

$$AirFlowRate = 1.82 \times 10^{-2} \times \lambda \times \frac{P_e}{V_c}(SLPM) \quad \text{(IV.1)}$$

Where λ is the stoichiometric ratio defined as the total amount of oxygen flow divided by the oxygen used. A good approximation for the minimum stoichiometric ratio to operate a fuel cell is 3 moles of oxygen for each mole of oxygen required. P_e is the power output in watts, and V_c is the average voltage across a cell. A value of 0.60 V can be used as an average voltage approximation if the value cannot be found through experimentation or is not given. This equation can be used for all fuel cells regardless of size as an estimate for air flow rate requirements [2].

2.2. Adsorptive filter breakthrough equations describing capacity, adsorption rate, breakthrough time, and inlet and outlet concentrations

Filter breakthrough equations are required to relate filter attributes to inlet and outlet air properties. The filter attributes include the chemical properties of sorbent capacity (N_0) and rate of adsorption (k'), and the footprint which includes area (A), thickness (L) and weight (m). Another attribute commonly used to describe filters is voidage (ε). The air properties are face velocity (v_0), inlet concentration (C_0), and outlet concentration (C_1). Several previously studied equations are effective at predicting breakthrough times for adsorbent beds.

An exact breakthrough equation for non-reversible adsorption onto a surface can be applied to a single or dual layer bed. Equation 2, derived by Neal Amundson [14], is based on mass balance across an adsorptive bed allowing for a time varying input concentration.

$$\frac{C}{C_0} = \frac{C_0\left(t - \varepsilon\, z/v_0\right)\exp\left[\varepsilon\frac{k}{v_0}\right]\int_0^{t-\varepsilon z/v_0} C_0(\eta)\,d\eta}{\exp\left[\varepsilon\frac{k}{v_0}\right]\int_0^{z}(N_0 - n(\xi))\,d\xi + \exp\left[\varepsilon\frac{k}{v_0}\right]\int_0^{t-\varepsilon z/v_0} C_0(\eta)\,d\eta - 1}, t \geq \varepsilon\frac{k}{v_0} \tag{IV.2}$$

This equation is then integrated resulting in the following equations which can be used to calculate the outlet concentration of a gas after passing through a single or double layer filter. A constant inlet concentration was used to integrate the outlet concentration of the first layer (C_1). C_1 was then inserted back into Equation 2 and integrated to calculate C_2.

$$C_1 = \frac{C_0}{1 + \left(e^{\varepsilon_1 k_1 C_0 \tau_1} - 1\right)e^{\varepsilon_1 k_1 C_0 (t - \varepsilon L_1 / v_0)}} \tag{IV.3}$$

$$C_2 = \frac{C_1\left[1 + e^{-\varepsilon_1 k_1 C_0 \tau_1}\left(e^{\varepsilon_1 k_1 C_0 (t - \varepsilon z_2 / v_0)} - 1\right)\right]^{\frac{\varepsilon_2 k_2}{\varepsilon_1 k_1}}}{\left(e^{\varepsilon_2 k_2 C_0 \tau_2} - 1\right) + \left[1 + e^{-\varepsilon_1 k_1 C_0 \tau_1}\left(e^{\varepsilon_1 k_1 C_0 (t - \varepsilon z_2 / v_0)} - 1\right)\right]^{\frac{\varepsilon_2 k_2}{\varepsilon_1 k_1}}} \tag{IV.4}$$

In Equation IV.4 $z_2 = L_1 + L_2$. Another equation used to determine outlet concentration from a single layer adsorptive bed, developed by Yoon and Nelson is based on probabilistic reasoning [6].

$$C_1 = \frac{C_0}{1 + e^{k'(\tau - t)}} \tag{IV.5}$$

Equation 5 allows for estimates to be made on the breakthrough constants used in the exact breakthrough equation. By using experimental data, a regression analysis yields values for k', ($k*C_o$). Also, from a breakthrough curve, saturation capacity (τ) in units of time can be read off at the time corresponding to $C = ½ C_o$. This allows for solving for capacity, N_0, in grams contaminant being removed per cm^3 sorbent, by using the following equation:

$$\tau = \frac{N_0 L}{v_0 C_0} \tag{IV.6}$$

Both the k' and N_0 can be used for a prediction of breakthrough concentration at different flow rates, inlet concentrations, and filter thicknesses. Face velocity is a function of flow rate and filter surface area. Inlet concentration and time are user inputs related to the operating environment of the fuel cell. Outlet concentration can be provided by the manufacturer or estimated based on experimental data on cathode durability.

2.3. Pressure drop relationships with filter thickness and air face velocity

Pressure drop (ΔP) has been correlated with face velocity, bed depth, viscosity (μ), void fraction, and gas density (ρ). Pressure drop through both packed beds and microfibrous beds is also related to particle diameter. However, in microfibrous beds there is an additional pressure drop related to fiber diameter.

The Ergun equation is commonly used to describe flow through packed beds [15].

$$\frac{\Delta P}{L} = 150\left(\frac{\mu v_o}{D_P^2}\right)\frac{(1-\varepsilon)^2}{\varepsilon^3} + \frac{7}{4}\left(\frac{\rho v_o^2}{D_P}\right)\frac{1-\varepsilon}{\varepsilon^3} \tag{IV.7}$$

In order to estimate the pressure drop across microfibrous materials (a high voidage mixture of fibers and particles), the Porous Media Permeability equation (PMP) is used to apply to beds that have porosity greater than 50%. This equation considers form drag losses which are small in low porosity material (e.g. packed beds).

PMP equation for high voidage microfibrous materials:

$$\frac{\Delta P}{L} = 72\left(\frac{\tau^2}{\cos^2(\Theta)}\right)\left(\frac{\mu v_o}{\varepsilon^3}\right)\left(\frac{1-\varepsilon}{\phi D}\right)^2\left(1+X_{FD}\right)+6\left(\frac{\tau^3}{\cos^3(\Theta)}\right)\left(\frac{\rho v_o^2}{2\varepsilon^3}\right)\frac{1-\varepsilon}{\phi D}\left(C_f+\frac{C_{FD}}{4}\varepsilon\right) \quad \text{(IV.8)}$$

In addition to the variables used in the Ergun Equation, the PMP equation uses tortuosity ($\tau = 1+0.5(1-\varepsilon)$), shape factor ($\varphi$), and the angle of flow paths through the bed (θ). The coefficient of drag is represented by C_D for a sphere (usually 0.6). The coefficient of friction for turbulent flow is C_f and the coefficient of form drag of a sphere in turbulent flow is C_{FD} ($C_{FD} = C_D - C_f$). Values corresponding to the Ergun equation can be found by equating the PMP equation to the Ergun and modified Ergun equations [15].

Empirical pressure drop relationships can also be determined experimentally by recording pressure drop as a function of layer thickness and flow rate. The advantage to this method is that it is more accurate; however, it prevents correlations to be made between properties of the filter such as the effects of particle size on pressure drop. An example empirical equation is:

$$P_2 - P_1 = C_1 L_1 v_0 + C_2 L_1 v_0^2 \quad \text{(IV.9)}$$

where C_1 and C_2 are constants solved for from data, v_0 is the face velocity and L_1 is the thickness of the layer. The second term in the equation accounts for inertial losses from a change in direction of air flow through the filter. An example of these types of losses

would occur when studying a pleated filter. In most cases, however, the losses are small and negligible.

2.4. Compressor power and efficiency

2.4.1. Compressor power

A study of the compressor is necessary to correlate the pressure ratio and power. A simple experimental setup consists of a pressure tap on each side of the compressor, a means of adding pressure drop to each side of the compressor (e.g. orifice plates), and a controller to operate the compressor. The compressor can be operated at different flow rates and pressure ratios while power provided to the compressor is recorded. Figure IV.3 shows the resulting plot for a 12V compressor used in this study.

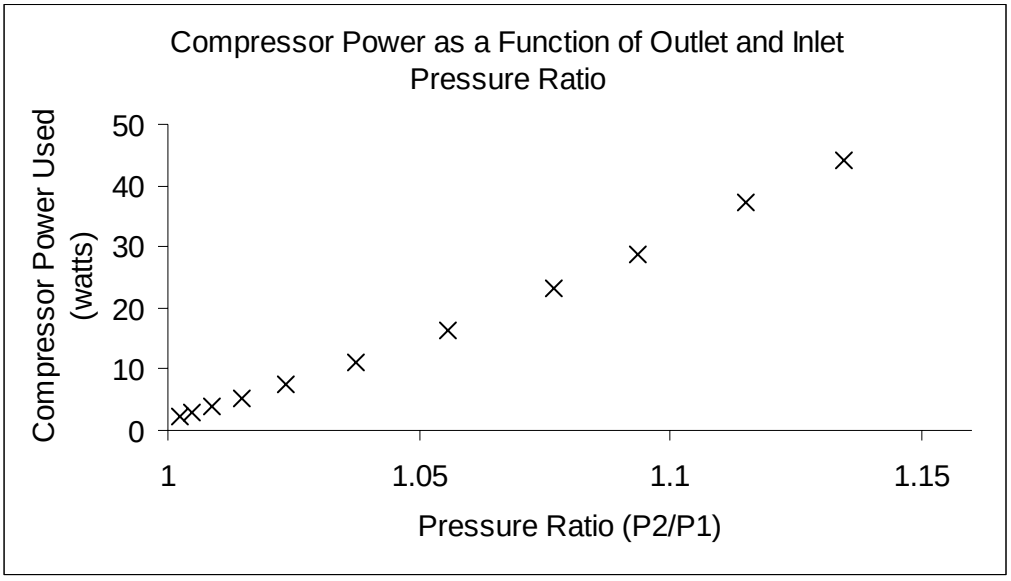

Figure IV.3: Power using a 12/64" Inlet Orifice and 11/64" Outlet Orifice.

In this case the correlation is linear and will be in the form,

$$CompressorPower = m\left(\frac{P_2}{P_1}\right) + b \qquad \text{(IV.10)}$$

2.4.2. Compressor efficiency

Several efficiency definitions exist that can be used to describe performance of a compressor. The most common efficiency equation, due to its accuracy and ease of determining input values, is specific overall efficiency.

$$\bar{\eta}_{overall,ad} = \frac{\dot{m}_e c_p T_1 \left[\left(\frac{P_2}{P_1}\right)^{\frac{k-1}{k}} - 1\right]}{\dot{W}_{shaft,e}} \qquad \text{(IV.11)}$$

In this case, m_e is the experimental mass flow at the discharge, T_1 is the ambient inlet temperature, P_2/P_1 is the pressure ratio, and k is a constant and is 1.4 for adiabatic [2]. A compressor study that yields efficiency measurements provides the ability to locate the surge line on a performance chart, identifiable as the points where efficiency approaches zero.

2.4.3. Compressor performance charts

Another method of obtaining data on compressors is with a performance curve. Centrifugal compressors have performance charts which give the efficiency and pressure ratios at which the compressor can be operated. On this chart, efficiency is represented by constant efficiency contours. Performance charts also show a surge line, which represents the point at which the compressor becomes unstable if operated at a higher

pressure ratio, at the same flow rate, or at a lower flow rate at the same pressure ratio. The surge line represents the point air flow through the compressor is unable to keep the compressor from overheating. This instability causes backflow and possible damage to the compressor. The performance chart is important in understanding the operating capabilities of the compressor, as well as to help understand power requirements [2].

3. Design algorithm

Using the previously discussed design equations and relationships, an algorithm was created to relate the design considerations to filter thickness and compressor parasitic power. The design equations were organized such that each variable could be solved starting with inputs that are readily available from the manufacturer or able to be experimentally determined. The linearity of the algorithm allows for a simple computer program to be built with few assumptions. A completed algorithm is shown in Figure IV.4.

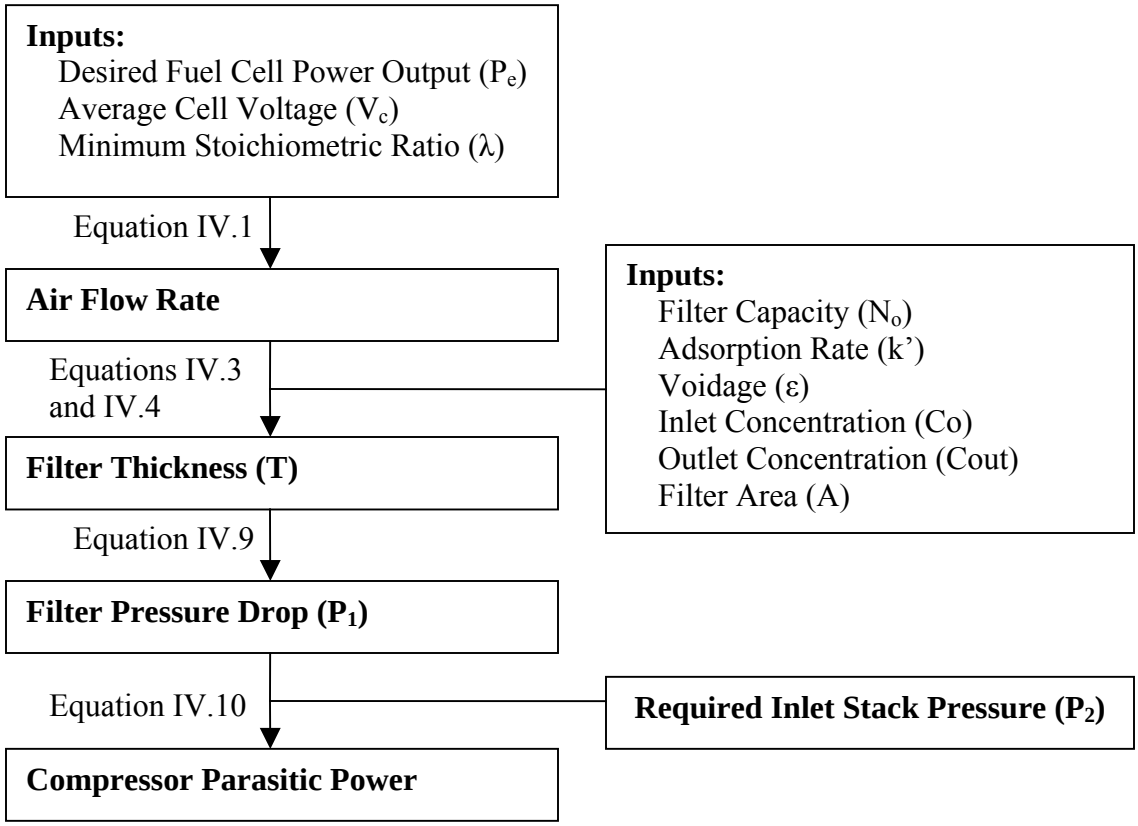

Figure IV.4: Final, programmable design algorithm

V. DESIGN ALGORITHM APPLICATION TO BALLARD FUEL CELL

1. Application overview

A study was performed, applying the filter design algorithm to a Ballard NEXA fuel cell. This study provides further detail on the algorithm through transgression of the individual steps of the algorithm and shows how the algorithm is applied to a real system. Application of the algorithm also allows for an analysis of the accuracy of assumptions and creation of recommendations for improvements. The results of this study show how predictions may be made comparing filter thickness, pressure drop and parasitic power requirements of the compressor.

The first step in applying the algorithm is choosing a filter type for study. Four different options are considered for application to the NEXA fuel cell; packed bed, a microfibrous sheet, a pleated microfibrous sheet, and a composite bed.

Other design considerations require a study of the compressor, required air flow rates by the stack, and pressure drops in the fuel cell. Inputs also include pressure drop relationships for filter materials and breakthrough constants for the filter options. For application to the NEXA fuel cell, each step will be discussed and compared with actual data to provide an understanding of where future improvements can be made. Once data has been collected, predictions are made about filter thickness, layer ratios in a composite bed, and power requirements to operate the compressor.

2. Filter design options and footprint

2.1. Filter design options

Filter design options include four different filter types; traditional packed bed, microfibrous materials, a composite bed, or a pleated microfibrous media filter. Each design option possesses unique attributes allowing for a filter design that is capable of being tailored to specific applications. Microfibrous materials have been proven effective at high log, low capacity removal. Microfibrous materials can also be pleated which reduces pressure drop across the filter. A packed bed has a low pressure drop and is effective at filtration requiring high capacity sorbents. However, these materials have poor contacting and are therefore poor at high log removal applications. By combining the two, a composite bed, provides another filter option capable of utilizing the strengths of microfibrous materials and packed beds to provide an overall thinner filter for high capacity high log removal applications.

2.2. Filter footprint

Physical size constraints may exist in the fuel cell system that need to be considered both before and after the filter design analysis. Filter area is required by the algorithm for calculation of face velocity and filter pressure drop. Filter thickness is an output by the algorithm. Thickness is studied at the end of the analysis to determine if the resulting filter thickness is feasible.

3. Air flow rate and stack pressure

3.1. Stack air flow requirements

Figure V.1 compares data taken on the NEXA FC with values predicted using the following equation.

$$AirFlow = 1.82 \times 10^{-2} \times \lambda \times \frac{P_e}{V_c}(SLPM) \qquad \text{(V.1)}$$

The Ballard manual suggests using 0.6 volts for average voltage across a cell. Typical stoichiometric ratios based on values given by the NEXA software at higher power outputs were about 2.7.

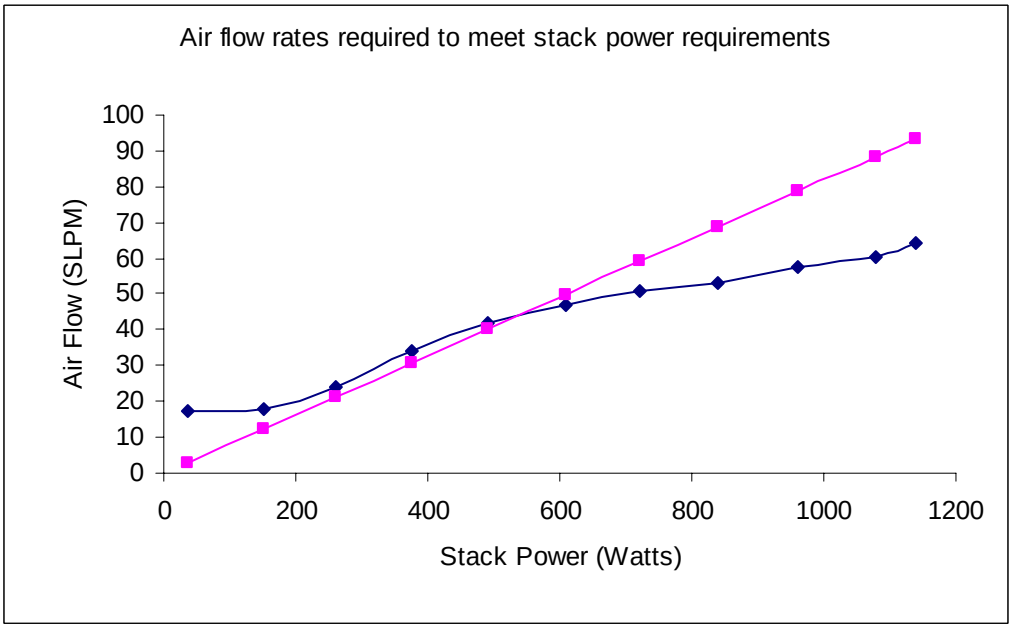

Figure V.1: Predicted air flow model compared with actual data

The results of the flow rate study using the fuel cell show a correlation between flow rate and power requirements that is nonlinear. Accuracy of the model is highest between 200 and 800 slpm. At low flow rates the flow rate is constant at around 20 SLPM. This is necessary in order to maintain membrane humidity and to prevent the

compressor from operating at low flow, inefficient levels. It is evident that either other factors are involved in oxidant flow control than stoichiometric ratio and average cell voltage or that either the stoichiometric ratio or average cell voltage are not constant. Overall, the predicative model for air flow rate offers an effective means of predicting air flow when no other experimental data from the fuel cell is known.

3.2. Stack inlet pressure requirements

In addition to flow rate, experimental data relating stack inlet pressure (same as the outlet pressure of the compressor) to flow rate must be obtained. This data is similar to an orifice plot, and can be modeled or a trend line can be used to describe the system. This pressure should be plotted under the same experimental setup that the fuel cell will be operated in; using the same intake manifolds and exhausts systems. A trend line of the data was taken, yielding the following flow-pressure relationship for the NEXA fuel cell:

$$P_2 = 0.005 \cdot Flow^2 + 0.2359 \cdot Flow \qquad \text{(V.2)}$$

Pressure is in "H_2O and flow rate is in SLPM. P_2 is necessary for calculation of a pressure ratio used in studying the compressor and predicting power loads required to operate the compressor.

4. Compressor data collection

A study is required in order to understand the effects that a pressure drop resulting from additional filtration will have on compressor performance. Two methods were used to study the compressor. The first required a testing apparatus capable of operating the compressor outside of the fuel cell system. The second method used to study the

compressor was performed using the Ballard NEXA fuel cell by adding an inlet air flow pressure drop and determining its effect on fuel cell and compressor performance. Both of these methods are outlined in the following sections.

4.1. A compressor study using a compressor testing apparatus

If a cathode air filter is designed to fit into an existing fuel cell system, design must consider the operating capabilities of the compressor and the effects that a resistance to flow will have on system performance. Compressor limitations may exist which limit the maximum flow restriction on the inlet or outlet air stream of the system. A study of compressor efficiency and parasitic power provides information for defining the compressor which allows for prediction of performance under different conditions. These predictions are inserted into the design algorithm and aid in optimization of cathode air filter design and comparison of different design options. If compressor data is not available from the compressor or fuel cell manufacturer, a set of experiments may be performed to collect the data necessary for compressor analysis. A data analysis of the compressor can then be used to create target filter thicknesses or maximum filter thickness and also to predict the required power output to provide required air flow rates at various filter thicknesses.

Data collection on the compressor is accomplished with a detailed study on the type and performance of the compressor. The most common type of compressor used in fuel cells is a centrifugal compressor. One helpful tool for understanding centrifugal compressors and quantitatively representing them is a compressor performance curve. Compressor performance curves are helpful tools for understanding how the compressor

operates by showing efficiencies as well as the surge line and other operating limits. In order to create a performance curve, an apparatus must be created which allows for the control of the power supplied to a compressor which will be operated at different flow rates and pressure ratios. The power provided to the compressor and thermodynamic analysis of the PV work allows for calculation of efficiencies at different operating points. This data analysis allows for the determination of the effect that pressure drop created by a cathode air filter will have on operation of and parasitic power consumed by the compressor.

A Ballard NEXA fuel cell uses a centrifugal compressor operated with a 12 volt 3-phase brushless DC motor. The advantages of brushless DC are its durability, operating efficiency, and few contacting parts. Brushless DC motors require a controller that converts DC power to a 3-phase output. Due to the complexity of the NEXA control board, it is difficult to accurately measure voltage and current values being supplied by the controller to the compressor.

An attempt was made at studying the wave forms leading from the controller to the compressor by using an oscilloscope. The monitor output from the oscilloscope was noisy and resulting in no reliable data able to be derived from this experiment. It was also difficult to determine the power supplied to the controller due to the inaccessibility of the wires leading from the power supply to the controller. For this reason, a controller was bread-boarded that was capable of operating the compressor separate from the NEXA fuel cell system. This allowed for measuring voltage and current supplied to the controller rather than in the three phase wires leading to the compressor.

During the experiments, outlet face velocity, total current and voltage to the compressor and controller, and compressor inlet and outlet gauge pressure were recorded. Pressure at the apparatus inlet and outlet was assumed to be 1 atmosphere. Compressor efficiency was calculated assuming adiabatic compressor efficiency. The efficiencies were also calculated based on the total power supplied to the controller and the compressor. This includes the efficiency of the controller, motor, and compressor.

Data points were collected starting at the lowest flow rate that the compressor could operate. At this point the compressor efficiency is zero. The power supplied to the compressor was then increased until face velocity increments of 10-15 fpm were observed. Values were recorded at each increment until the upper flow rate was reached. The upper flow rates and pressure ratios were set by the fact that the controller overheated at higher power loads. This limitation may exist in the fuel cell system and will be further investigated.

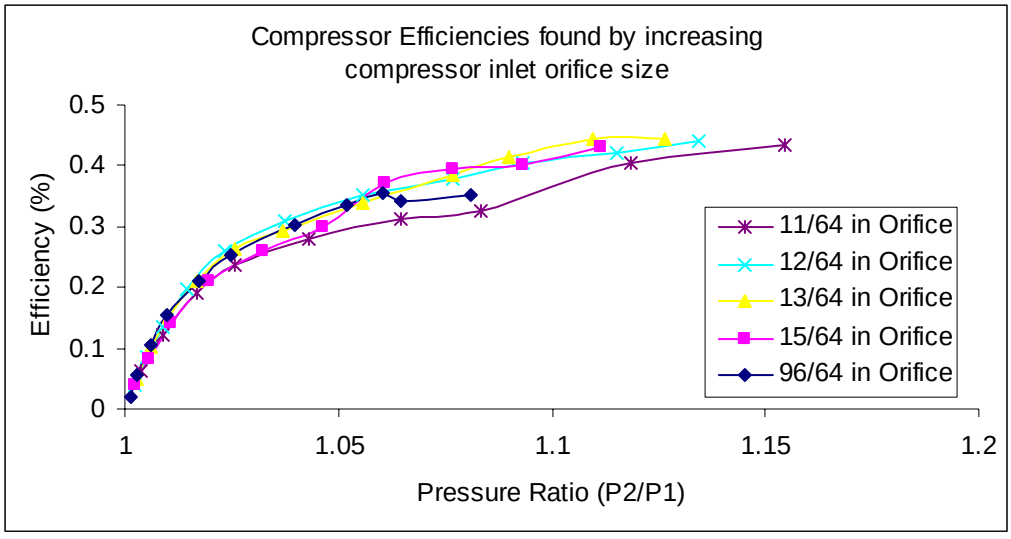

Figure V.2: Compressor efficiencies

The first observation from figure V.2 is that the efficiency of the compressor increases with the pressure ratio, at least up to a value of 1.15. Higher pressure ratios could not be reached with the current apparatus. This means that the upper operating regime cannot be studied and that the surge line cannot be found. The consequence of this is that the maximum filter pressure drop cannot be determined based on compressor data. However, it is possible to correlate the power requirements of the compressor to the inlet and outlet pressures. This correlation is shown in figure V.3.

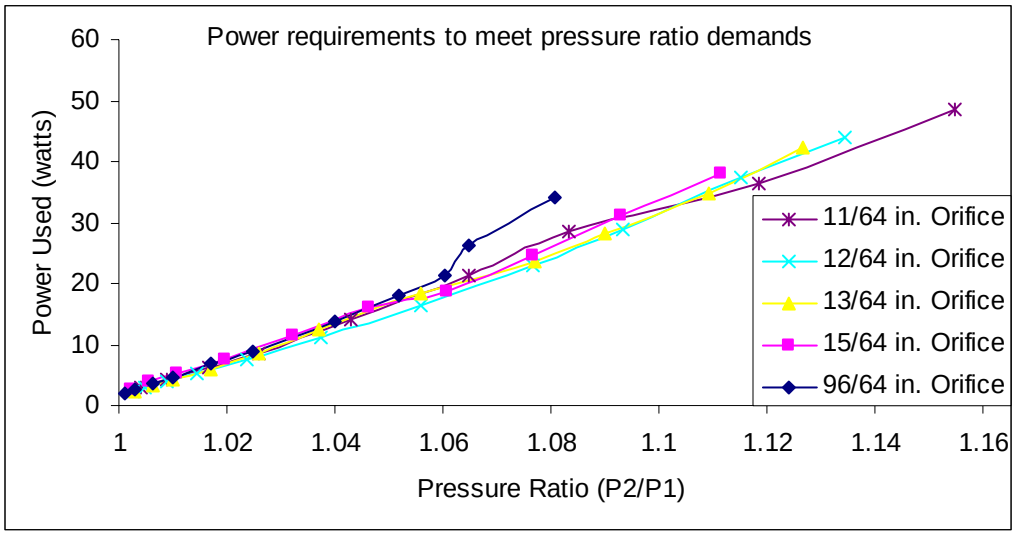

Figure V.3: Parasitic power required by the compressor to operate at given pressure ratios

Figure V.4 shows a linear correlation between total power and pressure ratio. A trend line representing the data can be regressed allowing for prediction of parasitic power used to operate the compressor a different pressure ratios that result from various filter thicknesses. This analysis results in the following equation for insertion in the algorithm program.

$$Power = 313.14 \cdot P_R - 312.74 \qquad \text{(V.3)}$$

4.2. A compressor study within the Ballard NEXA system

During experiments on the compressor using the testing apparatus, it was determined that higher pressure ratios could not be tested due to the possibility of over heating of the controller circuitry. A comparison between the possible limitation discovered using the apparatus and a possible limitation in the fuel cell could not be made due to the differences in the setup between the bread boarded controller and the controller used in the Ballard fuel cell. The possibility of the controller overheating brings to light the fact that limitations exist other than those measurable by the compressor testing apparatus. These limitations may be in the circuitry or arise when the compressor is operated within the fuel cell from a combination of factors. In order to further study possible system limitations, an in vitro study of the effect of restrictions placed on cathode air filter flow on system stability and performance was performed.

Operating limitations of the compressor may arise when the compressor is challenged within the fuel cell system by addition of a resistance to flow. A test for these limitations was designed to challenge the fuel cell allowing for the study of the effects of pressure drop on the compressor inlet on the fuel cell operating capability. This was accomplished by building five orifice plates with orifice sizes comparable to the ones used in the compressor studies. Orifice sizes of 10/64, 11/64, 12/64, 13/64, and 15/64" were drilled into plates the same size as the filter slot. The fuel cell was then operated on a load starting at 0 watts of output and increasing to 1200. A Dwyer manometer was used to measure pressure drop across the plate and the flow rate was measured by the flow detector built into the system and outputted onto the Ballard software.

The first test was done with the 15/64" orifice. The pressure drop across the stack was initially observed to be low when compared to the same orifice size and flow rate tested in the compressor testing apparatus. At high flow rates the pressure drop was still below 1" of water. The smaller, 11/64", orifice plate had the same results. To test this inconsistency the orifice was completely covered, blocking all air flow through the system intake that the filter would be set in. This brought about no noticeable effect on fuel cell performance as judged by changes in flow rate and stoichiometric ratio. After completely closing off the inlet the pressure drop only rose 0.2" of water.

The results of the in vitro tests lead to two possible conclusions. The Ballard manifold holding the compressor and intake filter contains leaks sufficient enough to completely bypass the intended inlet while causing little effect on the system or an intake bypass is built into the system. It is not this projects intent to pursue defects in the Ballard NEXA system. For this reason, the cathode air filter will be designed to optimize the breakthrough requirements and the filter effects on the power necessary to operate the compressor. Predictions will be made assuming that the fuel cell intake manifold does not leak.

5. Determination of Exact Breakthrough Equation Constants

For a breakthrough prediction values are needed for inputs into the following equations.

$$C_1 = \frac{C_0}{1+\left(e^{\varepsilon_1 k_1 C_0 \tau_1} - 1\right) e^{\varepsilon_1 k_1 C_0 (t - \varepsilon L_1 / v_0)}} \qquad \text{(V.4)}$$

$$C_2 = \frac{C_1\left[1 + e^{-\varepsilon_1 k_1 C_0 \tau_1}\left(e^{\varepsilon_1 k_1 C_0 (t-\varepsilon z_2 / v_0)} - 1\right)\right]^{\frac{\varepsilon_2 k_2}{\varepsilon_1 k_1}}}{\left(e^{\varepsilon_2 k_2 C_0 \tau_2} - 1\right) + \left[1 + e^{-\varepsilon_1 k_1 C_0 \tau_1}\left(e^{\varepsilon_1 k_1 C_0 (t-\varepsilon z_2 / v_0)} - 1\right)\right]^{\frac{\varepsilon_2 k_2}{\varepsilon_1 k_1}}} \qquad \text{(V.5)}$$

In many cases, k and C_o are lumped to form k'. This adsorption constant should be regressed from data at the same inlet concentration that other breakthrough estimates will be made. For this experiment, the inlet concentration will be 100 ppm and the k values will be solved for at this same concentration.

A recipe for a polymeric microfibrous materials sheet supporting activated carbon will be used that has been optimized for effective application as a polishing sorbent or pleated media. The sheet has a thickness of 0.4 centimeters with a basis weight of 870 g/cm^2. The volume percents of carbon, polymer, and cellulose are, respectively, 18.30%, 3.88%, and 0.62%. This leaves a voidage of 77.2%.

The packed bed used activated carbon from PICA, sized 12-30 mesh. The carbon has a voidage of 0.4. The packed bed was 5 cm in diameter and 0.95 cm thick. This resulted in a total carbon weight of 11.25 g.

The experiment resulted in the following breakthrough curves for the 0.4cm microfibrous supported carbon sheet and 0.95cm of packed bed. From Figure V.5, $\boldsymbol{\tau}$ values can be read as the time corresponding to an outlet concentration equal to ½ of the inlet concentration. Solving for N_0 in

$$\tau = \frac{N_0 T}{v_0 C_0} \qquad \text{(V.6)}$$

for a packed bed and microfibrous layer, values are 0.1 g/cm^3 and 0.04 g/cm^3 respectively.

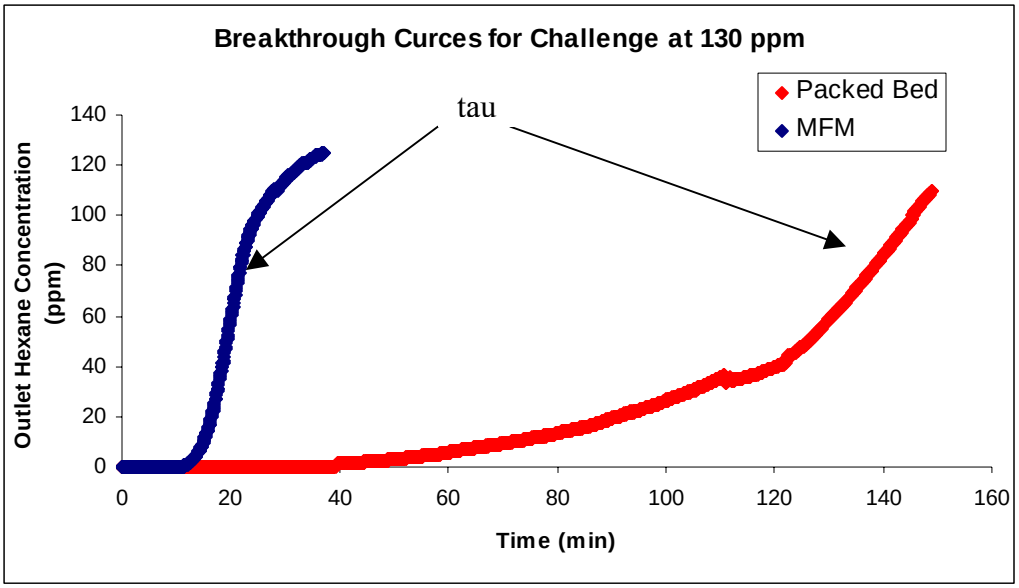

Figure V.4: Breakthrough curves for a 0.95 cm packed bed and a 0.4 cm microfibrous layer used to determine values for tau and capacity

Adsorption rate (k) values can also be determined from breakthrough data by solving Yoon and Nelson's breakthrough equation as a linear equation as follows.

$$\ln\left(\frac{C_0}{C}-1\right)=k'(\tau-t) \qquad \text{(V.7)}$$

By making the plot shown in figure V.6, and averaging the slope, an estimate of k' can be solved for. For the most accurate values, k' should be solved for at the concentration at which the filter will be tested at. However, a rough approximation of k' can be made by separating it into k*Co and solving for k.

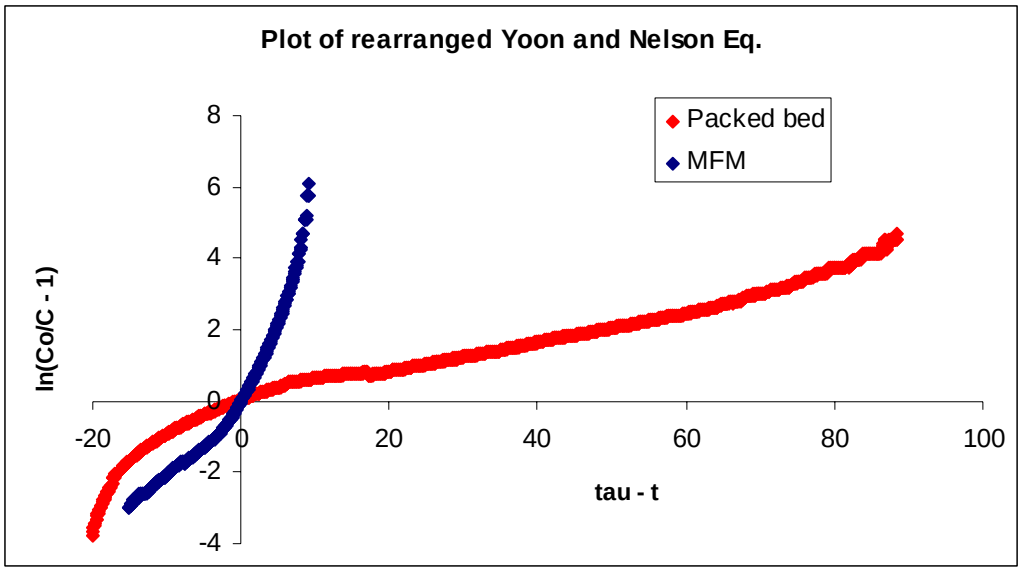

Figure V.5: A breakthrough equation that represents k' values as the slope

Adsorption rate constants for this case were determined to be 0.183 for a packed bed and 0.332 for microfibrous materials at 130 ppm hexane.

Table V.1
Values used in filter design algorithm

	Microfibrous Layer	**Packed Bed**
τ	65 min	140 min
Filter Capacity (N_o)	0.04 mols Hexane/cm^3 MFM	0.1 mols Hexane/cm^3 PB
Adsorption Rate (k')	0.00332*C_0	0.00183*C_0
Voidage (ε)	0.772	0.4

6. Determining filter pressure drop relationships

Several methods exist for predicting pressure drop across packed beds and microfibrous materials, including Ergun's equation and the porous media permeability equation. However, the simplest and most accurate method involves a simple experiment

involving recording pressure drop across a known thickness of the material being tested. The correlation is nearly linear; however, more data points should be taken at multiple face velocities to increase accuracy. The following plots show the results of a pressure drop experiment performed on 12-30 mesh PICA carbon and a polishing sorbent microfibrous media recipe.

The experiment was performed on the same apparatus used to test for breakthrough characteristics. Pressure drop was recorded from a 0-3 inch Dwyer manometer. A bed depth of 0.95 centimeters was used for the packed bed and 0.4 centimeters was used for the microfibrous sheet (corresponding to a basis weight on 870 g/m^2). The following plot shows the results of the experiment.

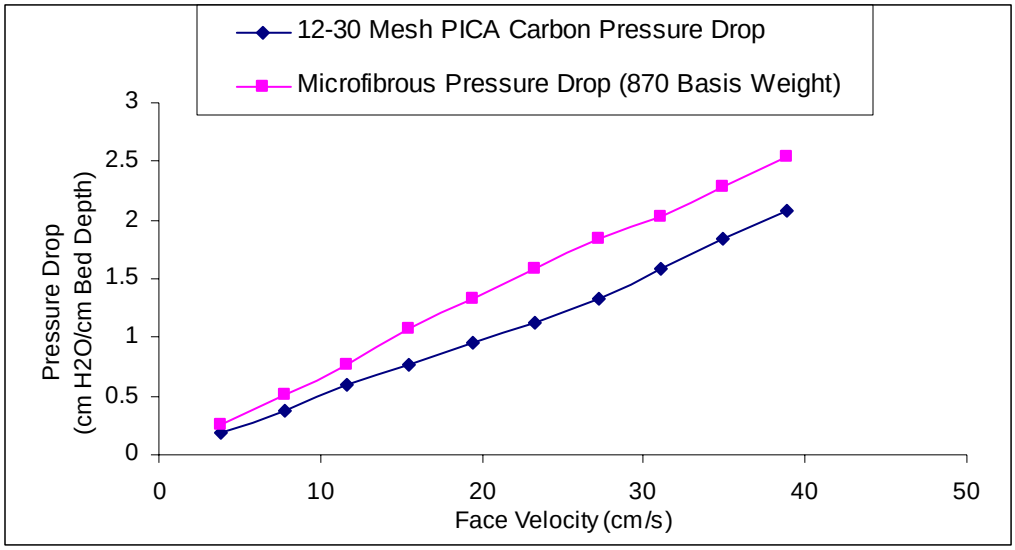

Figure V.6: Pressure drop as a function of face velocity for a 0.95 cm packed bed and a 0.4 cm microfibrous layer

This provides an estimate for pressure drop of each material:

$$dP_{MFM} = 0.0664 \cdot T_2 \cdot v_0 \quad \text{(V.8)}$$

$$dP_{PB} = 0.0514 \cdot T_2 \cdot v_0 \quad \text{(V.9)}$$

7. Filter design process results

The cathode air filter design algorithm was applied to a 1.2 kWe fuel cell in order to compare filter design options for removal of hexane with activated carbon. Hexane was used for this study because of its ease of use in the laboratory and well known adsorptive characteristics when used with activated carbon.

Four different design options were considered for this fuel cell application. The first three options were packed bed, microfibrous sheet, and composite bed. For these options a filter area of 55 cm^2 was studied for its ability to be retrofitted into the existing particulate filter location in the fuel cell when total thickness is less than 1 cm. The fourth design option, a pleated microfibrous materials filter, will be studied separate from the other filters. The pleated filter will be studied for the effects of breakthrough time and concentrations on the variable sheet thickness of the filter while the pleat depth is held constant at 1 cm, corresponding to the size required to retrofit the fuel cell.

In order to understand the effects of different inlet and outlet concentrations on the optimum filter designs, three case scenarios were studied. The three cases were:

Case I: 100 ppm to 5 ppm

Case II: 10 ppm to 0.1 ppm

Case III: 100 ppm to 0.1 ppm

Values shown in Table 2 were used to represent the fuel cell system and were obtained from the operating fuel cell manual.

Table V.2
Quantitative fuel cell attributes used in the algorithm

Input Parameter	**Parameter Value**
Fuel Cell Power Output (P_e)	1200 watts
Average Cell Voltage (V_c)	0.60 volts
Minimum Stoichiometric Ratio (λ)	2.7

The other inputs were experimentally determined. Breakthrough tests were performed on both 12-30 mesh activated carbon and a microfibrous polishing layer with a basis weight of 870 g/m^2 with 18.3% 60-140 mesh activated carbon. Values for k' and N_0 were regressed from experimental breakthrough data using the equation provided by Yoon and Nelson. Pressure drop relationships were determined in the lab as a function of thickness and flow rate. All resulting data used in describing the filter options are shown in Table 3.

Table V.3
Filter design input parameters collected from experimental data

Design Parameter	**Microfibrous Layer**	**Packed Bed**
Filter Capacity (N_o)	0.04 mols Hexane/cm^3	0.1 mols Hexane/cm^3
Adsorption Rate (k')	$0.00332*C_0$	$0.00183*C_0$
Voidage (ε)	0.772	0.4
Air Flow Rate	89.5 LPM	89.5 LPM
Pressure Drop	$0.0664*L_2*v_0$	$0.0514*L_1*v_0$
Compressor Power	$313.14 (P_2/P_1) – 312.74$	$313.14 (P_2/P_1) – 312.74$

The algorithm was used to predict an optimum filter thickness and the corresponding power requirements to operate the compressor. By varying the inlet concentration, outlet concentration, and breakthrough times, the different design options were studied under different capacity requirements and removal efficiency requirements.

7.1. Case I: Inlet Concentration of 100 ppm, Outlet Concentration of 5 ppm

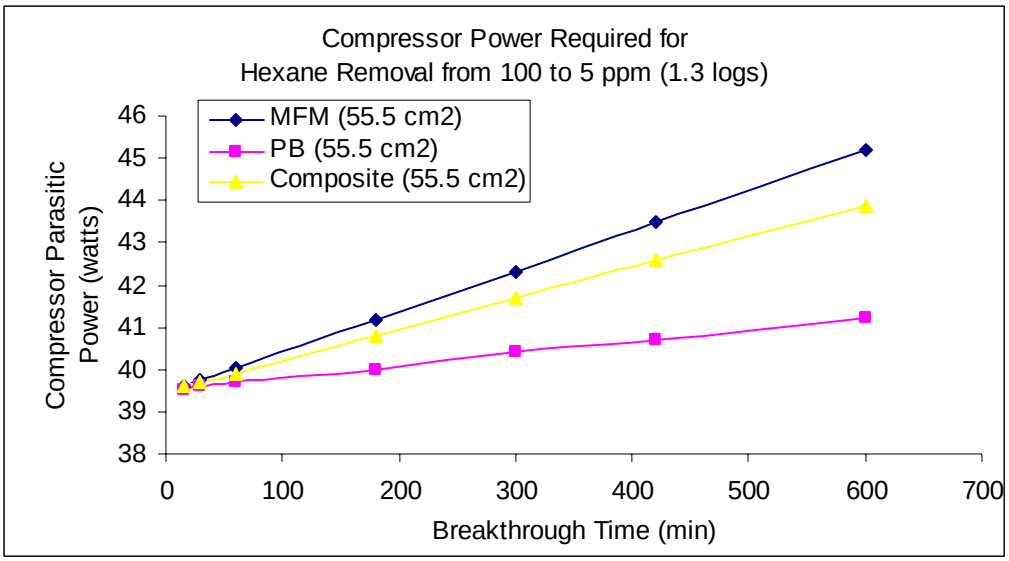

Figure V.7: Predicted power required to meet breakthrough time requirements

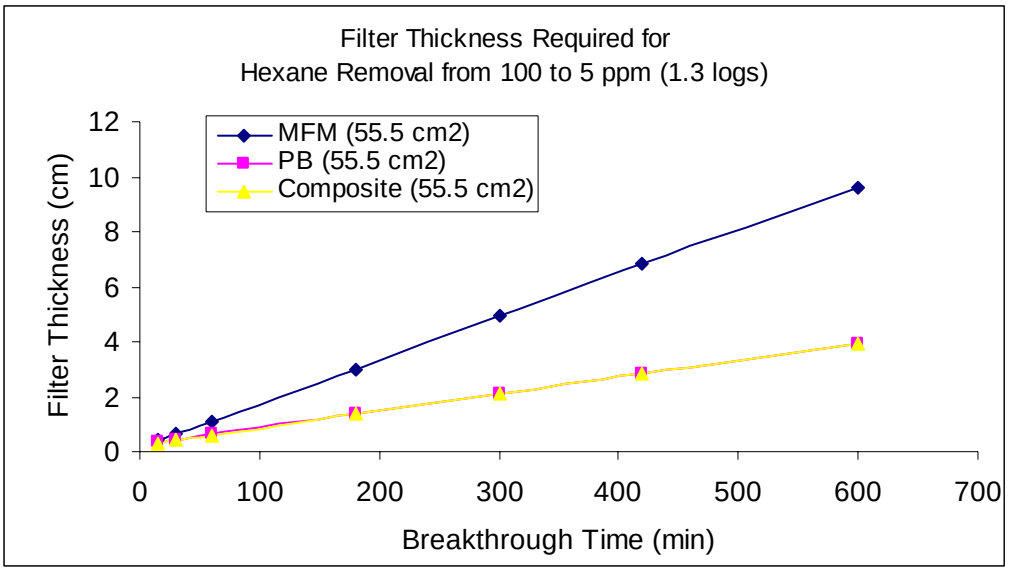

Figure V.8: Predicted thickness required to meet breakthrough time requirements

Figures V.7 and V.8 show the predicted thickness and compressor power requirements for different filter configurations optimized to meet breakthrough time requirements at an inlet concentration of 100 ppm and an outlet concentration of 5 ppm. This removal represents a 1.3 log removal and requires a high filter capacity. Because of the high capacity, the packed bed represents the best solution based on total filter thickness and pressure drop/compressor power. Because of the low logs of removal, microfibrous materials were not affective in reducing thickness or power requirements and therefore provided no benefit when used alone or in conjunction with a packed bed (composite bed).

7.2. Case II: Inlet Concentration of 10 ppm, Outlet Concentration of 0.1 ppm

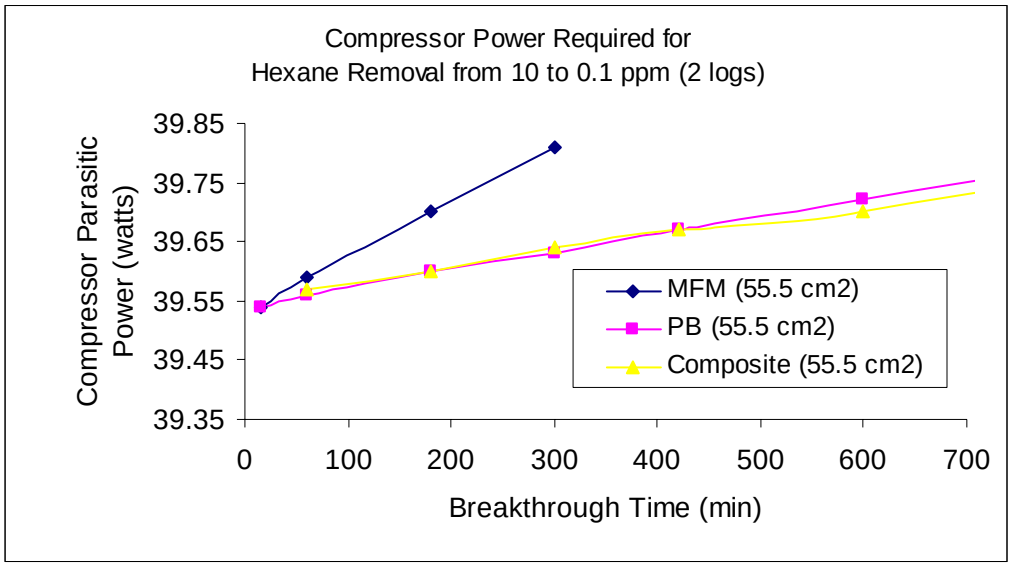

Figure V.9: Predicted power required to meet breakthrough time requirements

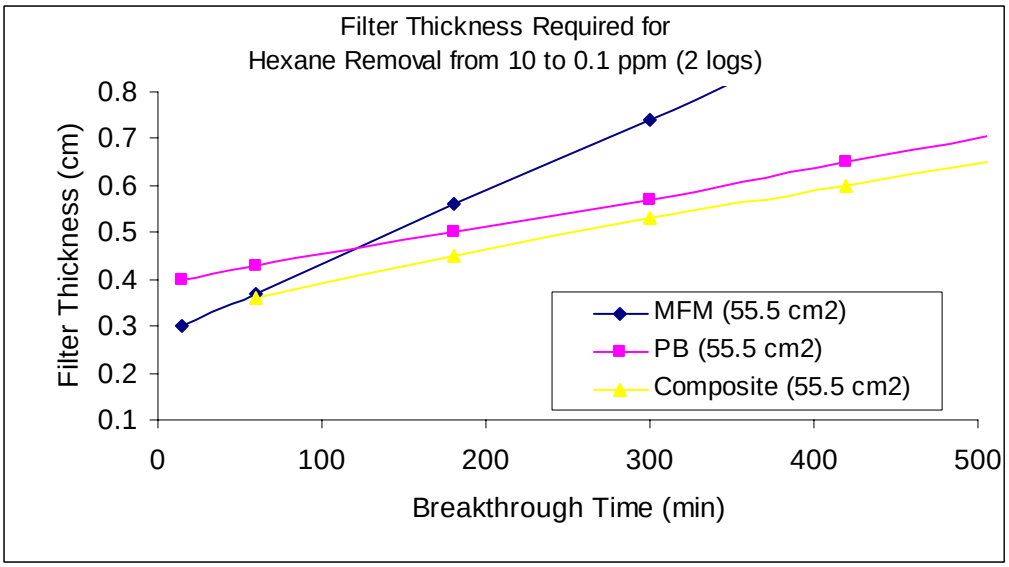

Figure V.10: Predicted thickness required to meet breakthrough time requirements

From Figure V.9 and Figure V.10 it is evident that microfibrous materials provide the thinnest filter option for a breakthrough time of less than 50 minutes; however, this solution also creates the most pressure drop, as evidenced by the increase in parasitic

power requirements. If, in practice, power requirements are the priority, then a composite bed provides the best solution. A composite bed also provides the best solution for higher breakthrough times. Figure 8 shows that a composite bed at the same thickness as a packed bed provides about a 100 minute longer breakthrough time.

7.3. Case III: Inlet Concentration of 100 ppm, Outlet Concentration of 0.1 ppm

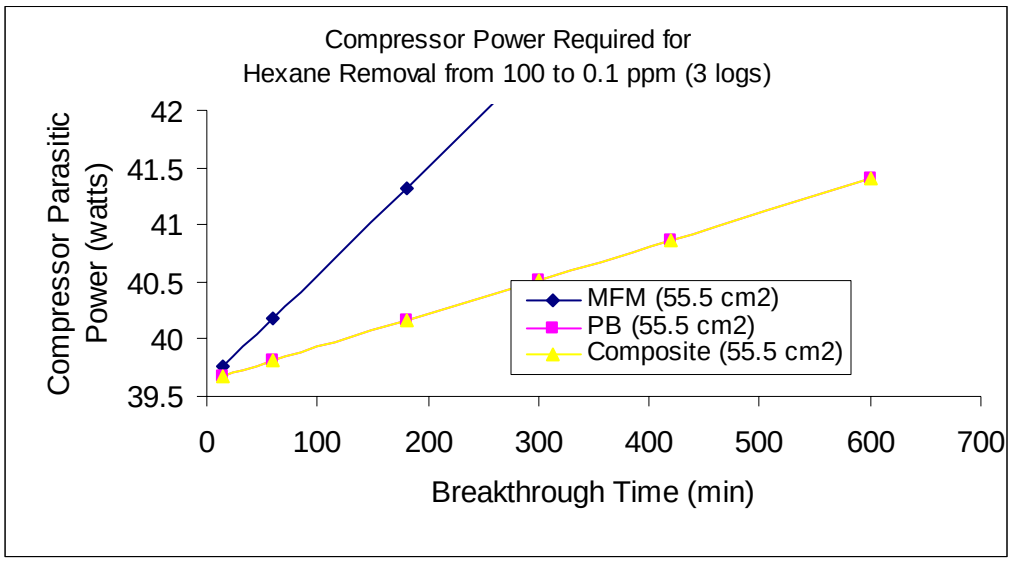

Figure V.11: Predicted power required to meet breakthrough time requirements

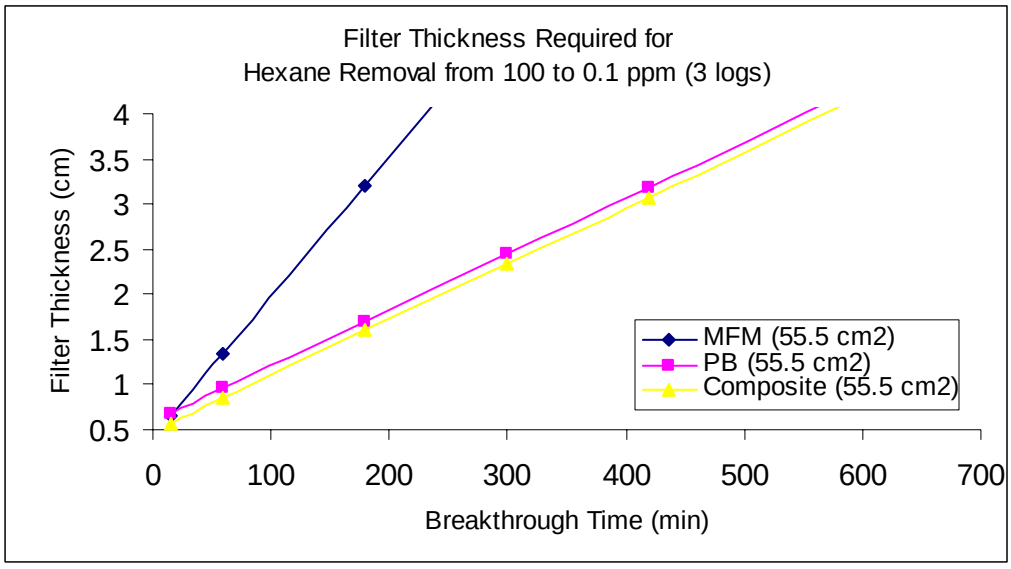

Figure V.12: Predicted thickness required to meet breakthrough time requirements

The third scenario, shown in Figure V.11 and Figure V.12, tests filter options under a situation that requires both a high capacity filter that is also capable of high logs of removal. In this situation, a composite bed outperforms the other design options by having a lower total thickness than the packed bed. It is also evident from Figure 10 that the addition of a microfibrous layer in place of a small length of packed bed to make a composite bed causes little additional pressure drop.

7.4. Case study for a pleated microfibrous filter

For an analysis of a pleated filter as a design option, a pleat depth of 1 cm was assumed and the thickness of the sheet was variable like the previous design options. This resulted in a constant filter thickness of 1 cm even though the sheet thickness was variable. Because of the pleats, a larger surface area was able to be fit into the same dimensions as the other options. A pleated microfibrous sheet was represented in the algorithm as having an area of 105.5 cm^2 (pleat factor of 1.9). This pleat factor was only

attainable at layer thicknesses less than 0.5 cm if it is still to fit in the 1 cm pleat depth, and will only be studied up to that thickness.

The Figure V.13 and Figure V.14 show the required sheet thickness and compressor power requirements if a pleated filter is used. The filter was only studied at an inlet concentration of 10 ppm and an outlet concentration of 1 ppm.

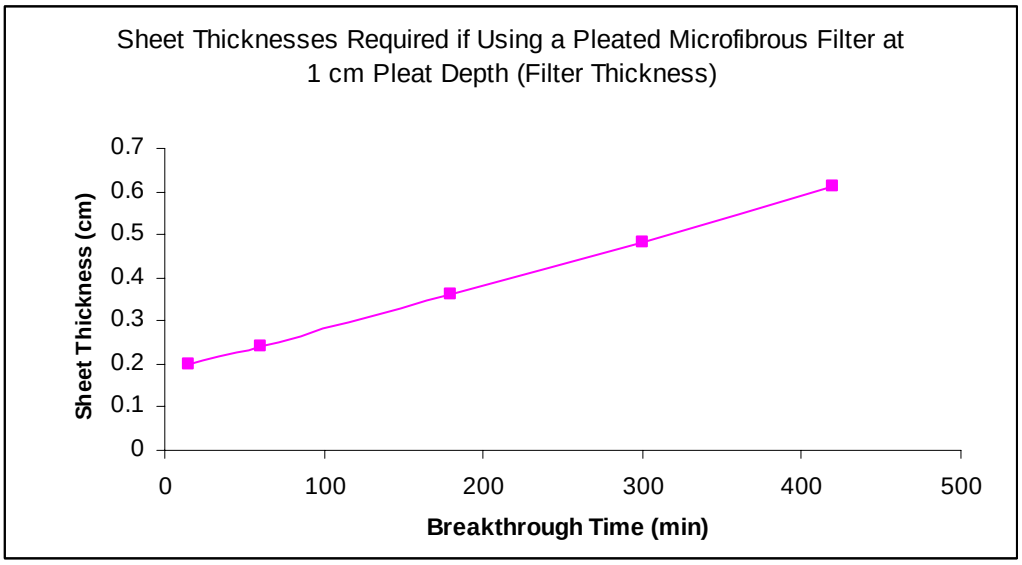

Figure V.13: Predicted sheet thickness of a microfibrous pleated filter at a challenge concentration of 10 ppm Hexane and an outlet concentration of 0.1 ppm

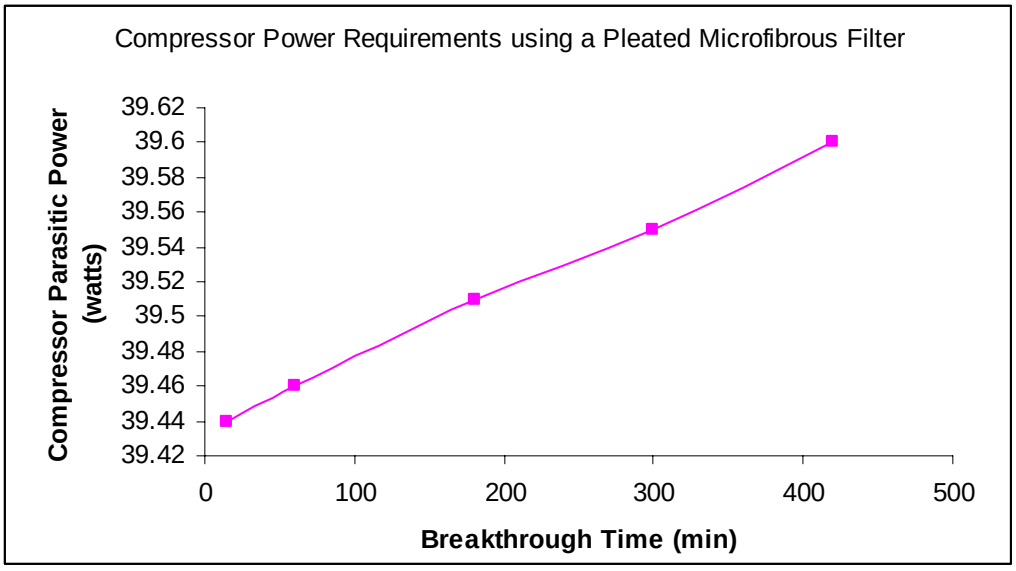

Figure V.14: Predicted compressor power requirements to operate a microfibrous pleated filter at a challenge concentration of 10 ppm Hexane and an outlet concentration of 0.1 ppm

An increase in sheet thickness results in only a small percentage increase in compressor power requirements from additional pressure drop. Pleated filters provide an additional solution for low capacity, high log removal applications. Another advantage to using a pleated filter rather than a packed or composite bed is the stability from the sinter locked network which adds resilience to the filter.

7.5. Detailed composite bed configuration analysis

For each case study and each breakthrough time tested, the composite bed was optimized to minimize total bed depth. This was accomplished by varying the thickness of the packed bed, calculating the required thickness of the microfibrous layer, and calculating the total thickness. Table 3 shows the individual layer thicknesses for each of the breakthrough times in the case study. By studying these graphs, information can be learned about the capacity and removal efficiency requirements of the filter and how

filter configurations are affected by inlet concentration, outlet concentration, and breakthrough time.

Case I and III require the thickest packed bed portion due to the fact that they have the higher capacity requirements of 95 and 99.9 ppm removal respectfully, when compared to case II, at 9.9 ppm removal. Secondly, the thickness of the microfibrous layer increases with log removal requirements. This is a result of the higher single pass removal efficiency required for high log removal.

Table V.4
Predicted, optimized individual layer thicknesses of the packed bed (L_1) and microfibrous layer (L_2) used to create a composite bed

	Case I 100 – 5 ppm 1.3 logs removal		**Case II** 10 – 0.1 ppm 2 logs removal		**Case III** 100 – 0.1 ppm 3 logs removal	
Time (min)	L_1 (cm)	L_2 (cm)	L_1 (cm)	L_2 (cm)	L_1 (cm)	L_2 (cm)
15	0.2	0.12	N/A	N/A	0.2	0.37
60	0.52	0.09	0.09	0.27	0.51	0.34
180	1.26	0.09	0.23	0.22	1.25	0.34
300	2	0.09	0.32	0.21	2	0.34
420	2.74	0.09	0.4	0.2	2.74	0.34
600	3.86	0.09	0.5	0.2	3.85	0.34
6000	37.29	0.09	3.86	0.2	37.28	0.34

Further analysis is performed by transgressing down the columns and by increasing breakthrough time requirements. By increasing breakthrough time, additional capacity is required to meet the breakthrough requirements. This results in an increase in the packed bed layer of the filter. However, at low breakthrough times, where capacity is less significant, a thicker microfibrous layer provides a shorter overall bed depth by reducing the critical bed depth (the minimum bed depth required to prevent immediate breakthrough).

VI. FILTER CONSTRUCTION AND TEST RESULTS

1. Filter Construction

Two cathode air filters were constructed to fit into a Ballard NEXA fuel cell. Breakthrough and pressure drop tests on these filters allowed for comparing results from tests with values predicted using the design algorithm. By making these comparisons, recommendations could be made on how the algorithm can be further modified to add detail and accuracy in its predictions.

For this test, filters will be constructed to fit into the Ballard NEXA fuel cell. The filters were tested at an inlet concentration of 100 ppm so that data can be compared with algorithm predictions from cases I and III. The filters were made of the same materials used to determine values for the algorithm. Tables V.1 and V.2 show the values used for predicting the filter performance.

Table VI.1
Quantitative fuel attributes used in the algorithm

Input Parameter	**Parameter Value**
Fuel Cell Power Output (P_e)	1200 watts
Average Cell Voltage (V_c)	0.60 volts
Minimum Stoichiometric Ratio (λ)	2.7

Table VI.2
Filter design input parameters collected from experimental data

Design Parameter	**Microfibrous Layer**	**Packed Bed**
Filter Capacity (N_o)	0.04 mols Hexane/cm^3	0.1 mols Hexane/cm^3
Adsorption Rate (k')	$0.00183*C_0$	$0.00332*C_0$
Voidage (ε)	0.4	0.772
Air Flow Rate	89.5 LPM	89.5 LPM
Pressure Drop	$0.0664*L_2*v_0$	$0.0514*L_1*v_0$
Compressor Power	$313.14 (P_2/P_1) – 312.74$	$313.14 (P_2/P_1) – 312.74$

The following sections describe the filter construction methods, testing results, and recommendations for improvements to the algorithm.

1.1. Filter frames

Two filters were constructed to retrofit into the existing slot for cathode air filters in the Ballard NEXA system. The first one is a composite bed design, and the second, a pleated microfibrous materials sheet. The filters are 5.87 cm high, 10.5 cm wide, and 1 cm thick. Aluminum, 1/32" thick, was used for the framing. The dimensions for the four parts (2 sides, and a top and bottom) are shown in figure XXX.

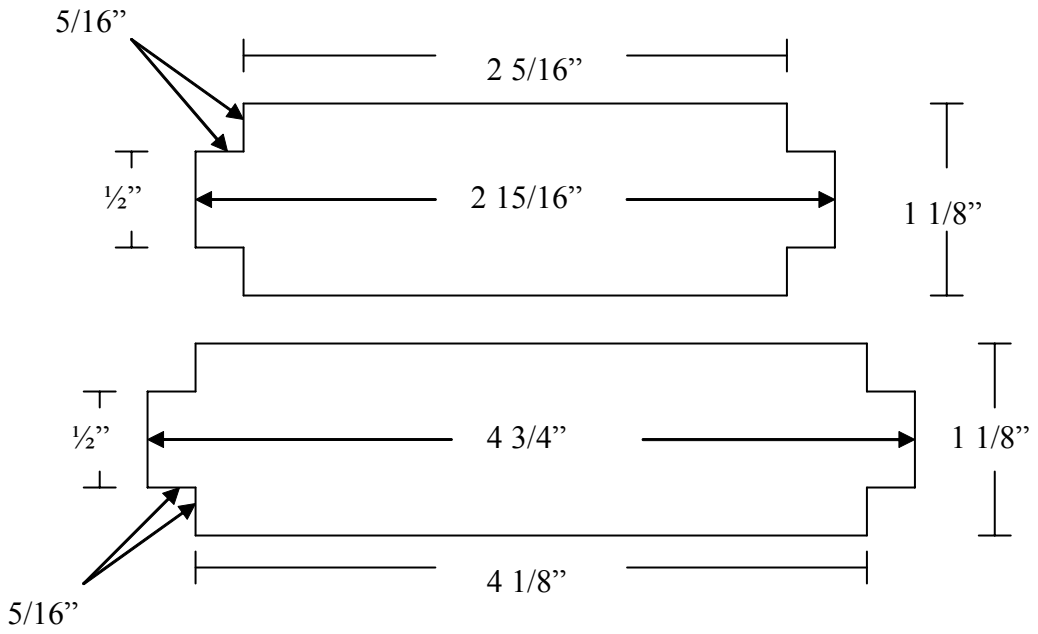

Figure VI.1: Cut metal frame dimensions used for constructing a cathode air filter

A metal brake was used to accomplish all of the bends. All four sides of the larger piece are bent towards the same direction at 90^{o} angles to make an open box. The smaller piece has only the long sides bent. The unbent tabs of the smaller pieces slide inside of the ends of the larger piece creating the filter frame.

1.2. Adsorbent materials

Microfibrous sheets were made on a one square foot paper making machine. The basis weight used was 870 g/m^2. The final filter was 18.3% by weight 60-140 mesh PICA activated carbon. The resulting filter had a thickness of 0.4 cm. The packed was comprised of 12-30 mesh PICA activated carbon.

1.3. Final Filter Design

Figure VI.2 shows the optimized filter thickness for a composite bed plotted at different breakthrough times. This plot predicts a 100 minute breakthrough for an optimized 1.2 cm composite bed. The thicknesses of the individual layers to make the composite bed are shown in Table VI.3.

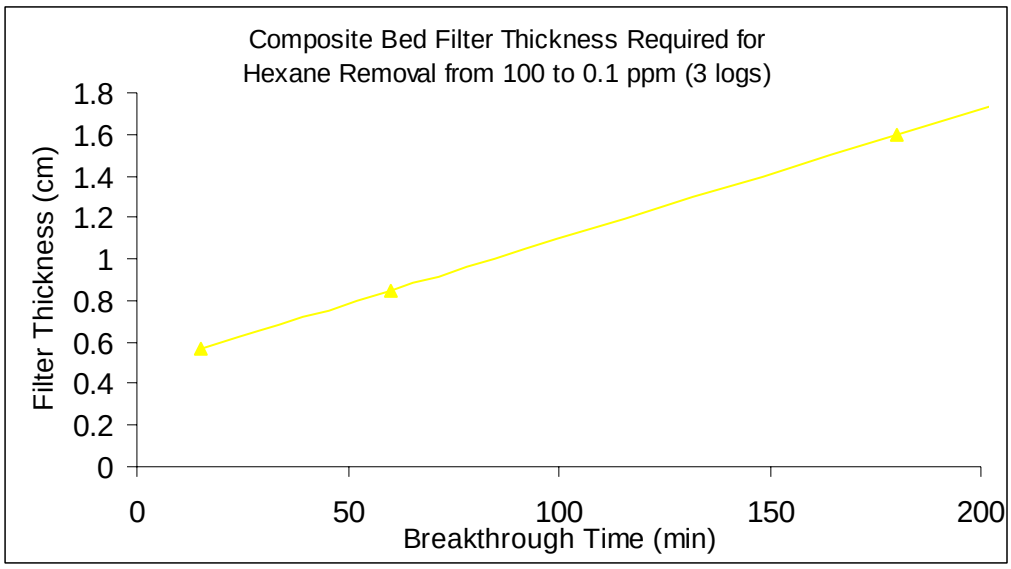

Figure VI.2: Predicted composite bed thickness required for hexane removal used to design a composite bed filter

Table VI.3
Values of layer thicknesses for optimized composite bed

	100-.1 (3 log)	
minutes	L_1	L_2
15	0.2	0.37
60	0.51	0.34
180	1.25	0.34
300	2	0.34
420	2.74	0.34
600	3.85	0.34
6000	37.28	0.34

The optimized composite bed configuration in this case has a packed bed of about .9 cm and a microfibrous bed of about 0.34 cm. The filter that will be constructed will utilize a 0.8 cm packed bed and a 0.4 cm microfibrous polishing layer.

Through a hands on trial and error process it was determined that a maximum basis weight of about 870 g/m^2, at a thickness of about 0.4 cm, can be pleated to fit into a filter 1.2 cm thick. For this reason, the same sheet used in the composite bed was used in a microfibrous pleated filter.

The following pictures show the construction materials for the composite bed as well as a final filter.

Figure VI.3: Materials of construction for composite bed cathode air filter

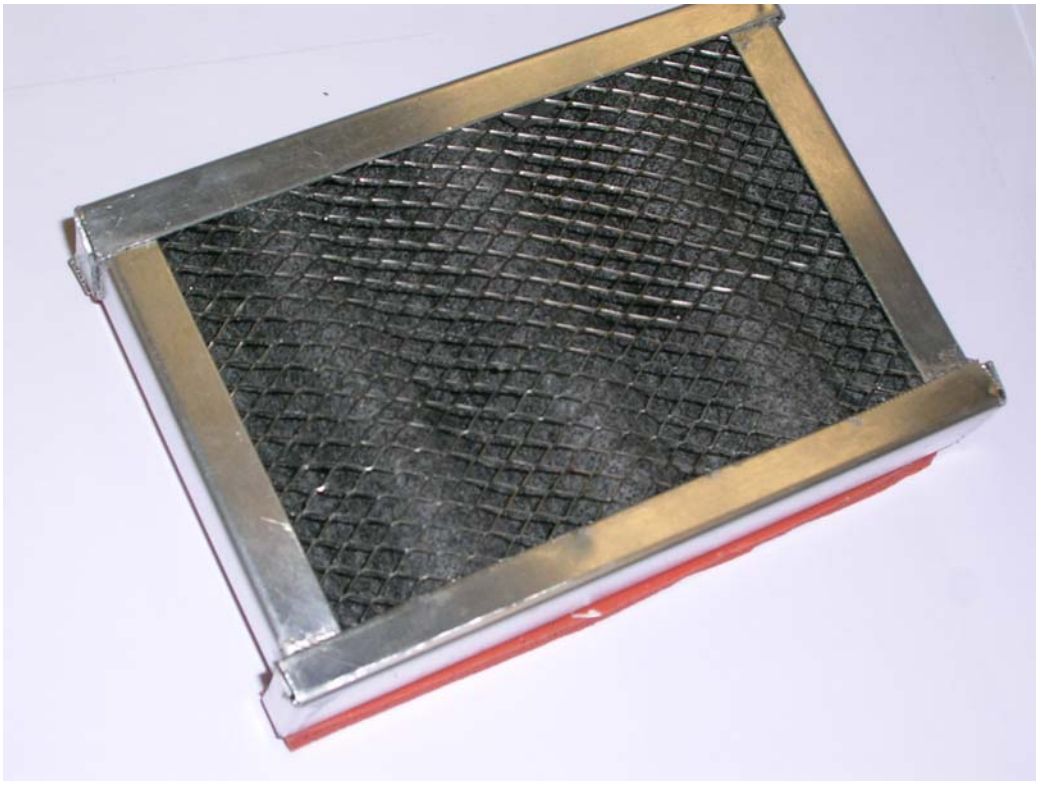

Figure VI.4: Picture of pleated cathode air filter

2. Filter Tests Results

2.1. Composite Bed Filter

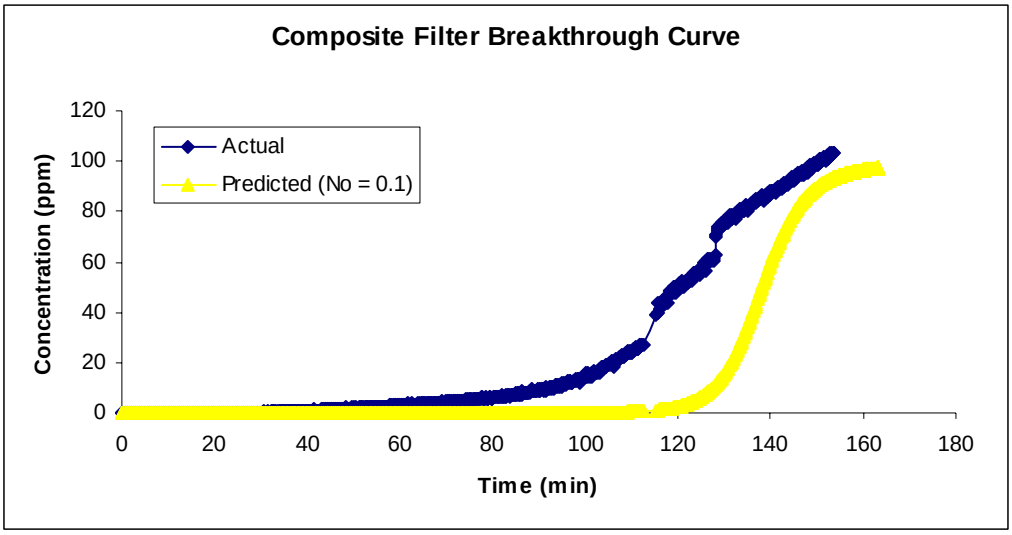

Figure VI.5: Actual breakthrough curves for composite bed compared to a predicted breakthrough curve by the algorithm

Figure VI.5 shows the results of the 100 ppm challenge breakthrough test on the composite bed filter. Breakthrough at 0.1 ppm was 27 minutes. Predicted value was 100 minutes. The predicted curve shows a sharper breakthrough. A shallower breakthrough curve results from a lower contacting efficiency than predicted. Since contacting efficiency is primarily a factor of adsorption rates the inaccuracy in the breakthrough curve is caused by inaccuracy in the determination of the adsorption rate values. The filter capacity is only slightly overestimated by the algorithm and as a result the breakthrough is sooner than predicted.

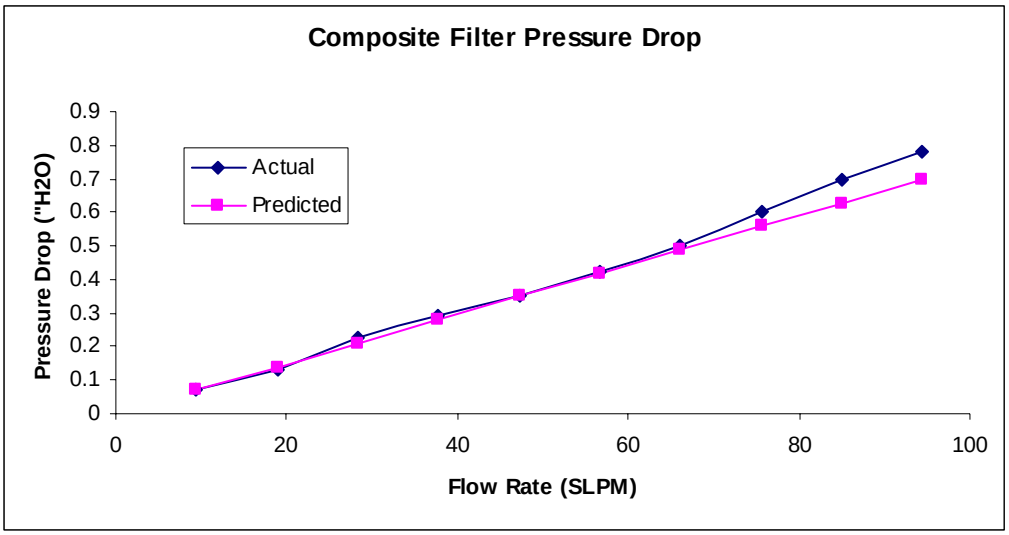

Figure VI.6: Pressure drop comparison between a composite bed filter and values predicted by the algorithm

Pressure drop predictions, shown in Figure VI.6, were accurate at flow rates lower than 70 slpm when compared to experimentally determined data. At higher flow rates actual pressure drop was higher than predicted. This may be due to inertial losses which cause a non-linear pressure drop relationship when operating at higher flow rates and was assumed negligible when the pressure drop formula was determined for a packed bed.

2.2. Pleated Microfibrous Filter

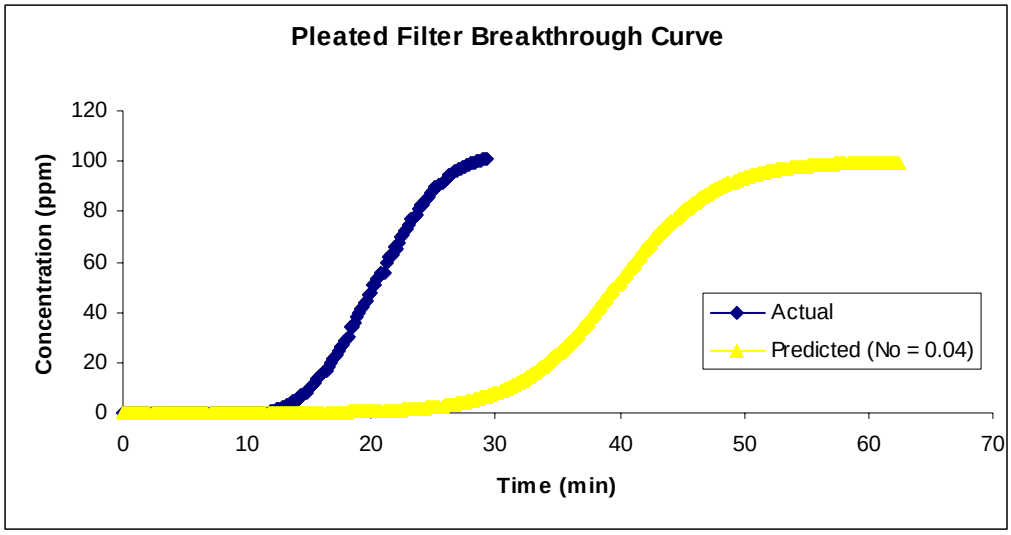

Figure VI.7: Actual breakthrough curves for a pleated filter compared to a predicted breakthrough curve by the algorithm

Figure VI.7 shows breakthrough curves predicted by the algorithm compared with those found experimentally. In this case, the breakthrough was 15 minutes sooner than predicted, indicating that the capacity was overestimated. Adsorption rate values were more accurate, evident by the similar shape of the sigmoidal breakthrough curve for both the actual and predicted curves.

Pressure drop predictions for the pleated filter, shown in Figure VI.8, are higher than actual values. A small percentage of this drop in pressure drop is a result of leaks in the filter and can be resolved with better construction techniques. A small curvature in the actual pressure drop is the result of inertial losses due to the air having to pass through the pleats. Inertial losses were assumed negligible in original pressure drop

calculations used to predict the pressure drop; therefore, the predictions were less accurate.

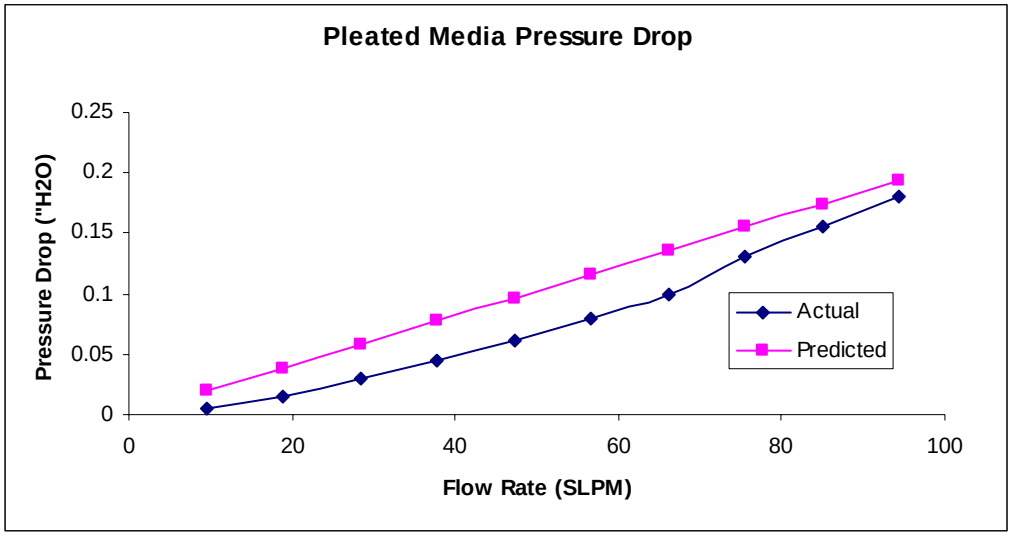

Figure VI.8: Pressure drop comparison between a microfibrous pleated filter and values predicted by the algorithm

Pressure drop predictions for the pleated filter are higher than actual values. This results from a higher surface area of the constructed filter that estimated when making the pressure drop predictions. The area above the lips of the filter was not accounted for when calculating the filter pressure drop. This effect was not significant in the composite bed because the lip seals off air flow from reaching this space. However, in a pleated filter air may move under the lip and into the area covered by the frame, pass through the media, and move back under the lip on the other side.

3. Recommendations for Improvement to Algorithm

The current algorithm assumes that the adsorption rate (k) is constant and obtains a value based on an average from data collected at one inlet concentration. This value is then used to calculate k values for other concentrations. A more accurate model of k could provide more accurate estimates on filter performance; however, this complicates the algorithm adding a new dimension to the program. Currently, the algorithm is kept one dimensional by solving for the concentration only at the exit of the filter leaving time as the only variable. A more accurate estimate of k would be calculated at an infinite number of points moving through the filter (perpendicular to the face) and at all points in time. In other words, k is a function of distance into the filter and time. A more accurate k estimate is increasingly important as filter thickness is increased due to the fact that there is a wider range of adsorption rate values through the filter. A well modeled adsorption rate also allows for a larger range of estimating filter performance while using less experimental data. This decreases the time necessary to design multiple filters for different applications using the same algorithm inputs.

Improvements to the understanding and modeling of pleated media would make the algorithm for accurate for pleated design. These changes could be made in both the pressure drop estimates and the breakthrough predictions. Pressure drop across pleated media contains inertial losses caused by a change in direction of flow of the bulk fluid. This causes an uneven distribution of pressure drop across the filter. An uneven pressure drop distribution may result in an uneven flow regime causing some areas to be challenged at a higher flow rate; hence, experiencing breakthrough at an earlier time.

VII. CONCLUSIONS AND FINAL COMMENTS

Optimization of a cathode air filter design to a variety of different fuel cell applications involves inputting design considerations into an algorithm predicting compressor power and filter breakthrough characteristics, both of which reflect fuel cell performance and net power output. Results from application of a programmable design algorithm to a 1.2kWe fuel cell show that the algorithm and design methodology are effective means of predicting filter effects on compressor power requirements. The predictions also show trends useful in tailoring a filter to specific requirements of an application.

Microfibrous materials provide the lowest pressure drop for cases requiring high log removal due to their high contacting efficiency. Packed beds have the lowest pressure drop for applications requiring a high capacity. However, the bed depth of a packed bed becomes large when meeting high log removal requirements. An optimized composite bed provides the most favorable solution for cases requiring both high contacting efficiency and high capacity. A filter must be optimized for each contaminant type and concentration to achieve the required operating life of the fuel cell and to minimize pressure drop which can consume as much as 1% of total output power. Use of a design algorithm provides a means of optimization by comparing the effectiveness of

different filter configurations, ultimately yielding higher fuel cell efficiency and operating life.

REFERENCES

1. Moore, Jon M., Lakeman J. Barry, Mepsted, Gary O. "Development of a PEM Fuel Cell Powered Portable Field Generator for the Dismounted Soldier" Journal of Power Sources 106 (2002) 16-20
2. Larminie, James and Dicks, Andrew. "Fuel Cell Systems Explained", SAE International; 2nd edition, May 2003, Chapter 1 and Appendix A 2.2.
3. Moore, Jon M., Adcock, Paul L., Lakeman, J. Barry, and Mepsted, Gary O. "The effects of Battlefield Contaminants on PEMFC Performance" Journal of Power Sources 85 (2000) 254-260
4. Costamagna, Paola and Srinivasan, Supramaniam. "Quantum Jumps in the PEMFC Science and Technology from 1960s to the Year 2000: Part I. Fundamental Scientific Aspects". Journal of Power Sources 102 (2001) 242-252
5. Mohtadi, R., Lee W. and Van Zee, J.W. "Assessing Durability of Cathodes Exposed to Common Air Impurities" Journal of Power Sources 138 (2004) 216-225
6. Cahela, Donald R., and Bruce J. Tatarchuk. "Design of Polishing Filter Adsorbents Using Sintered Microfibrous Metallic Networks as Carriers for High Effectiveness Sorbent Particulates." Proceedings of the AIChE 2003 Annual Meeting, Nov. 16 – 21, 2003: Fundamentals of Adsorption and Ion Exchange II. San Francisco, CA.

7. Cacciola, G., Antonucci, V., Freni, S., "Technology up date and new strategies on fuel cells" Journal of Power Sources 100 (2001) 67-79

8. Ballard NEXA Fuel Cell Manual, Ballard Power Systems, Inc (2003)

9. Hoogers, Gregory. "Fuel Cell Technology Handbook" CRC Press LLC 2003 1-5

10. Jakobert, B.J., Veldhuis, Frank A de Bruijn, and Ronald K.A.M. Mallant. "Air Pollution: A Problem for the SPFC Cathode?" 1998 Fuel cell seminar, Palm Springs, California, USA, 16-19 November 1998

11. Ruthven, Douglas M. Principles of Adsorption and Adsorption Processes. New York: Wiley-Interscience, 1984.

12. Harris, Daniel K., Cahela, Donald R., Tatarchuk, Bruce J. "Wet Layup and Sintering of Metal-Containing Microfibrous Composites for Chemical Processing Opportunities." Composites: Part A 32 (2001) 117-1126

13. Queen, Andy "High Efficiency Adsorbent Filters via Packed Bed + Polishing Sorbent Architectures for Regenerable Collective Protection Equipment"

14. Amundson, Neal R. "A Note on the Mathematics of Adsorption in Beds" J.Phys Colloid Chem. 52 (1948) 1153-1157

15. Tatarchuk, Bruce J. and Cahela, Donald R. "Permeadbility of Sintered Microfibrous Composites for Heterogeneous Catalysis and Other Chemical Processing Opportunities." Catalysis Today 69 (2001) 33-39

16. Ueno, K., Bye, R.E., Hunter, K.S., VAIREX Corporation, "Compressor Efficiency Definitions" May 2003. http://www.vairex.com/pdf/Efficiency-0523.pdf

17. Jakobert, B.J., Veldhuis, Frank A de Bruijn, and Ronald K.A.M. Mallant. "Air Pollution: A Problem for the SPFC Cathode?" 1998 Fuel cell seminar, Palm Springs, California, USA, 16-19 November 1998
18. Mohtadi, R., Lee W. and Van Zee, J.W. "Assessing Durability of Cathodes Exposed to Common Air Impurities" Journal of Power Sources 138 (2004) 216-225
19. Kosanovic, Lisa. "Running on Air" Mechanical Engineering January (2004) 40-42
20. Costamagna, Paola and Srinivasan, Supramaniam. "Quantum Jumps in the PEMFC Science and Technology from 1960s to the Year 2000: Part I. Fundamental Scientific Aspects". Journal of Power Sources 102 (2001) 242-252
21. Lister S., McLean, G. "PEM fuel cell electrodes" Journal of Power Sources130 (2004) 61-76
22. Ashley, Steven. "On the road to fuel cell cars" Scientific American March 2005 62-69
23. Betournay, Marc C., Bonnell, Gary, Edwardson, Eric, Paktunc, Dogan, Kaufman, Arthur, Lomma, A. Timothy. "The effects of mine conditions on the performance of a PEM fuel cell." Journal of Power Sources 134 (2004) 80-87
24. Qi, Zhigang, He, Chunzhi, Kaufman, Arthur. "Effect of CO in the anode fuel on the performance of PEM fuel cell cathode" Journal of Power Sources 111 (2002) 239-247

APPENDIX A. AIR FLOW DERIVATION

Referenced from Fuel Cell Systems Explained

Starting with:

$$charge = 4F \times O_2$$

$$O_2 = \frac{I}{4F}\left(\frac{moles}{s}\right)$$

For multiple stacks:

$$O_2 = \frac{I \times n}{4 \times F}\left(\frac{moles}{s}\right)$$

To substitute in for current:

$$P_e = V_c \times I \times n$$

$$I = \frac{P_e}{V_c \times n}$$

Substituting for current and converting from moles/s to kg/s

$$O_2 = \frac{32 \times 10^{-3} \times P_e}{4 \times V_c \times F}\left(\frac{kg}{s}\right)$$

Dividing by 0.21 to find total air flow, converting to the more commonly used units of SLPM and multiplying by the stoichiometric ratio (λ = (total oxygen supplied)/(total oxygen used by FC)):

$$AirFlow = 1.82 \times 10^{-2} \times \lambda \times \frac{P_e}{V_c}(SLPM)$$

APPENDIX B. SAMPLE MAPLE OUTPUT FOR A COMPOSITE BED

```
> restart;
> Coppm := 100; #ppm

                        Coppm := 100

> Coutppm := 5; #ppm

                        Coutppm := 5

> Co := Coppm/(1000000*22.4*1000); #mol/cm3

                                    -8
                    Co := .4464285714 10

> Cout := Coutppm/(1000000*22.4*1000); #mol/cm3

                                    -9
                    Cout := .2232142857 10

> BT := 2*60; #in minutes

                        BT := 120

> Area := 55.5; #sq cm

                        Area := 55.5

> stoic := 2.7; #Minimum Stoichiometric Ratio Required

                        stoic := 2.7

> Vcell := 0.60; #Average Voltage Across a Cell  FROM BALLARD MANUAL

                        Vcell := .60

> FCPower := 1200; #Operating Power Output
```

FCPower := 1200

> O2used := 3.48E-3*FCPower/Vcell; #in SLPM

O2used := 6.960000000

> AirFlow := O2used*stoic/0.21; #AirFlow in SLPM
>

AirFlow := 89.48571429

> AirFlowKg := AirFlow*2.38*10^(-5); #AirFlow in kg/s

AirFlowKg := .002129760000

> P2 := 0.6453*AirFlow - 7.1332; #AirFlow to Stack Inlet Pressure #in "H2O

P2 := 50.61193143

> P1 := (406.782-((406.782+P2)/1.135))*2.54; #cm H2O

P1 := 9.6310501

> vo := AirFlow*1000/(Area*60); #cm/sec

vo := 26.87258687

> dP2 := 0.0664*T2*vo; #cm of H2O

dP2 := 1.784339768 T2

> dP1 := 0.0514*T1*vo; #cm of H2O

dP1 := 1.381250965 T1

> solve(dP1+dP2 = P1, T2);

-.7740963855 T1 + 5.397542706

> T2 := %;

T2 := -.7740963855 T1 + 5.397542706

```
> plot(T2, T1=0..5, 0..5, labels = ["Thickness of Packed Bed (cm)", "Total Thickness of
MFM (cm)"], font=[COURIER, 12], labeldirections=[HORIZONTAL,VERTICAL],
numpoints=1000);

> vo :=AirFlow*1000/Area; #cm/min

                        vo := 1612.355212

> tau1 := 0.1*T11/(vo*Co*86);

                    tau1 := 161.5432595 T11

> tau2 := 0.04*T22/(vo*Co*86);

                    tau2 := 64.61730377 T22

> k1 := 0.183;

                          k1 := .183

> k2 := 0.332;

                          k2 := .332

> epsilon1 := 0.4;

                        epsilon1 := .4

> epsilon2 := 0.772;

                        epsilon2 := .772

> Conc1 := Co/(1+(exp(epsilon1*k1*tau1)-1)*exp(-epsilon1*k1*BT));

                      -8
  Conc1 := .4464285714 10

                           1
        ------------------------------------------------
        .9998468358 + .0001531642014 exp(11.82496660 T11)

> Conc2 := (Conc1*(1+exp(-epsilon1*k1*tau1)*(exp(epsilon1*k1*BT)-
1))^((epsilon2*k2)/(epsilon1*k1)))/((exp(epsilon2*k2*tau2)-1)+(1+exp(-
epsilon1*k1*tau1)*(exp(epsilon1*k1*BT)-1))^((epsilon2*k2)/(epsilon1*k1)));
>
```

```
                    -8
  Conc2 := .4464285714 10

                                    3.501420765   /
       (1 + 6527.940774 exp(-11.82496660 T11))           /  (
                                                  /

       (.9998468358 + .0001531642014 exp(11.82496660 T11)) (

       exp(16.56167343 T22) - 1

                                      3.501420765
        + (1 + 6527.940774 exp(-11.82496660 T11))          ))

> solve(Cout = Conc2, T22);

                          /
                          |
                          |             13               14
  .06038037184 ln(-.3333333333 \-.4999234179 10   - .9500076582 10

                                      /700284153\
                                      |---------|
                                      \200000000/
       (1. + 6527.940774 exp(-11.82496660 T11))

                  9                             9
        - .765821007 10  exp(11.82496660 T11) + .765821007 10

       exp(11.82496660 T11)

                                      /700284153\\
                                      |---------||
                                      \200000000/|   /
       (1. + 6527.940774 exp(-11.82496660 T11))          /  /  (
                                                  /

                 13              9
       .1666411393 10   + .255273669 10  exp(11.82496660 T11)))

> T22 := %;

                                 /
                                 |
```

```
                          |            13
T22 := .06038037184 ln(-.3333333333 \-.4999234179 10   -

            14
     .9500076582 10

                                  /700284153\
                                  |---------|
                                  \200000000/
     (1. + 6527.940774 exp(-11.82496660 T11))

              9                           9
      - .765821007 10  exp(11.82496660 T11) + .765821007 10

     exp(11.82496660 T11)

                                  /700284153\\
                                  |---------||
                                  \200000000/|   /
     (1. + 6527.940774 exp(-11.82496660 T11))          / /  (
                                             /

            13             9
     .1666411393 10   + .255273669 10  exp(11.82496660 T11)))
```

```
> plot(T22, T11=0..2, numpoints=1000, labels = ["Thickness of Packed Bed (cm)",
"Thickness of MFM (cm)"], font=[COURIER, 12],
labeldirections=[HORIZONTAL,VERTICAL]);
```

```
> T11 := T1;
```

```
                     T11 := T1
```

```
> plot([T22 , T2], T1=0..5, 0..8, labels = ["Thickness of Packed Bed (cm)", "Total
Thickness of MFM (cm)"], font=[COURIER, 12],
labeldirections=[HORIZONTAL,VERTICAL], numpoints=1000);
```

```
> Ttotal2 := T22+T1;
```

```
                                 /
                                 |
                                 |            13
Ttotal2 := .06038037184 ln(-.3333333333 \-.4999234179 10   -

            14
```

```
      .9500076582 10

                                    /700284153\
                                    |---------|
                                    \200000000/
      (1. + 6527.940774 exp(-11.82496660 T1))

                  9                              9
       - .765821007 10  exp(11.82496660 T1) + .765821007 10

      exp(11.82496660 T1)

                                    /700284153\\
                                    |---------||
                                    \200000000/|   /
      (1. + 6527.940774 exp(-11.82496660 T1))          /  /  (
                                                      /

                 13               9
      .1666411393 10   + .255273669 10  exp(11.82496660 T1))) + T1
```

```
> Ttotal1:= T2+T1;

            Ttotal1 := .2259036145 T1 + 5.397542706
```

```
> plot([Ttotal1, Ttotal2], T1=0..6, 0..6, labels = ["Thickness of Packed Bed (cm)", "Total
Thickness of Composite (cm)"], font=[COURIER, 12],
labeldirections=[HORIZONTAL,VERTICAL], numpoints=1000);
```

```
> Ttotaldiff := diff(Ttotal2, T1);

                        /            /
                        |            |
                        |            |
  Ttotaldiff := -.1811411155 |-.3333333333 \
                        \

                                    /500284153\
                                    |---------|
                 20                 \200000000/
      .2567719253 10   (1. + 6527.940774 %2)          %2

                   10                 10
       - .9055807829 10   %1 + .9055807829 10   %1 %3
```

```
                                    /500284153\   \
                                    |---------|   |
                15                  \200000000/   |
      - .2069892097 10   %1 (1. + 6527.940774 %2)          %2/

        /             13              9
       /  (.1666411393 10   + .255273669 10  %1) +
      /

              10              13              14
      .1006200870 10   (-.4999234179 10   - .9500076582 10   %3

                9               9           /
      - .765821007 10  %1 + .765821007 10  %1 %3) %1  /
                                          /

                                    \
                                    |
                13              9   2|
      (.1666411393 10   + .255273669 10  %1) |
                                    /

                13              9      /              13
      (.1666411393 10   + .255273669 10  %1)  /  (-.4999234179 10
                                    /

                  14                9
      - .9500076582 10   %3 - .765821007 10  %1

                9
      + .765821007 10  %1 %3) + 1

  %1 := exp(11.82496660 T1)

  %2 := exp(-11.82496660 T1)

                      /700284153\
                      |---------|
                      \200000000/
  %3 := (1. + 6527.940774 %2)

> fsolve(0=Ttotaldiff, T1);

                      .8901518117
```

> T1:=%;

T1 := .8901518117

> T2 := T22;

T2 := .09063040950

> Ptotal := dP1+dP2;

Ptotal := 1.391238493

> Pratio := (406.782+P2)/(406.782-Ptotal);

Pratio := 1.128279119

> Tpower := 303.56*Pratio - 302.13; #Watts

Tpower := 40.3704094